Limitation of fixed nitrogen and deepening of the carbonate-compensation depth through the Hirnantian at Dob's Linn, Scotland

Matthew C. Koehler[1*], Eva E. Stüeken[2], Stephen Hillier[3,4], and Tony Prave[2]
[1]*Department of Earth & Space Sciences and Astrobiology Program, University of Washington, Seattle WA 98195-1310, USA*
[2]*School of Earth and Environmental Sciences, University of St. Andrews, St. Andrews KY16 9AL, Scotland*
[3]*The James Hutton Institute, Craigiebuckler, Aberdeen AB15 8QH, United Kingdom*
[4]*Department of Soil and Environment, Swedish University of Agricultural Sciences, P.O. Box 7014, SE-75007 Uppsala, Sweden*

*Corresponding Author: matthew.koehler@globalviral.org

Abstract

The late Ordovician is characterized by dramatic changes in global climate concurrent with a major mass extinction and possible changes in ocean redox. To further refine our understanding of these events, we present nitrogen and carbon isotope and abundance data from the Ordovician-Silurian (O-S) Global Boundary Stratotype Section and Point at Dob's Linn, Scotland. We show that this section experienced post-depositional ammonium migration from the organic-rich to the organic-poor horizons. However, our data suggest that isotopic fractionations from ammonium substitution into illitic clay minerals are small and can be corrected. Reconstructed primary nitrogen isotope ratios indicate that unlike in tropical continental shelf sections that were transiently enriched in nitrate during the Hirnantian glaciation, the sub-tropical continental slope setting at Dob's Linn experienced persistent limitation of fixed nitrogen across the O-S boundary. Shallow subpolar settings appear to be the only environment that show persistent nitrate availability at that time. This pattern suggests that spatial trends in marine nitrate concentrations – which are observed in the modern ocean as a result of latitudinal temperature gradients – were already established during the Paleozoic. While the average marine O_2 chemocline depth may have deepened during the Hirnantian glaciation, it probably did not lead to global ventilation of the deep ocean, which may have been delayed until the Carboniferous. Furthermore, carbonate data from this and other sections suggest a deepening of the carbonate compensation depth (CCD) during the Hirnantian. This observation indicates that Pacific-style responses of the CCD to glacial/interglacial periods were operational across the O-S boundary, and that the expansion of abiotic carbonate deposition and preservation beyond the shelf break could have in-part mediated changes to surface CO_2 during these extreme changes in climate.

Keywords: Nitrogen Isotopes, Paleozoic Nitrogen Cycling, Abiogenic Carbonate Storage, Ammonium Migration, Nitrogen in Clay

1. Introduction

The Ordovician-Silurian (O-S) boundary is characterized by dramatic changes in Earth's climate, surface environments, and biosphere, but linkages and spatial patterns in these

perturbations are still a subject of debate (Algeo et al., 2016). Through the Ordovician it is generally thought that atmospheric pCO_2 levels and surface temperatures steadily decreased from greenhouse conditions (Finnegan et al., 2011; Nardin et al., 2011; Trotter et al., 2008), reaching a low in the end-Ordovician Hirnantian glaciation. This model is supported by the carbon isotope record which indicates periods of enhanced organic carbon burial in the Ordovician, possibly caused by increases in marine primary productivity (e.g. Bergström et al., 2009). Carbon burial, and perhaps enhanced weathering of flood basalts and volcanic arc materials (Ernst and Youbi, 2017; Young et al., 2009), would have led to increased CO_2 sequestration from the atmosphere and associated cooling. It has been proposed that this cooling trend may have favored partial or episodic ventilation of the oceans resulting from changes in ocean circulation associated with stronger latitudinal temperature gradients (Kah et al., 2016). This may have caused deep-ocean anoxia to diminish – and is a process that has been used in part to explain the Great Ordovician Biodiversification Event (GOBE; Marenco et al., 2016).

The onset of the largest positive carbon isotope excursion in the Ordovician is documented from the early Hirnantian glacial stage with a peak in the late Hirnantian (e.g. Fan et al., 2009; Melchin and Holmden, 2006; Underwood et al., 1997), consistent with rapid CO_2 drawdown and global cooling. Various sedimentary sections from across the O-S boundary also record transient increases in carbonate deposition during the early to middle Hirnantian (Chen et al., 1999; Finney et al., 2007; Finney and Perry, 1991; Yan et al., 2009), hinting at additional carbon storage in sediments beyond the continental shelf (this study). The initiation of the Hirnantian glacial period likely occurred when pCO_2 levels fell below a threshold (Gibbs et al., 1997; Herrmann et al., 2004), eventually resulting in the expansion of a Gondwanan ice sheet to volumes that rivaled or surpassed those of the Pleistocene Last Glacial Maximum (Finnegan et al., 2011). The beginning and end of the glaciation were associated with pulses of extinction (Jablonski, 1991).

Here, we present nitrogen and carbon isotope and abundance data from the O-S Global Boundary Stratotype Section and Point at Dob's Linn, Scotland. This is the first nitrogen isotope dataset from subtropics across the O-S boundary, and it is one of two sections deposited beyond the continental shelf break recording $\delta^{15}N$ values and transient increases in carbonate abundances during the Hirnantian. We also compile over 2300 $\delta^{15}N$ measurements of Paleozoic sedimentary rocks from the literature to better contextualize broad changes to global nitrogen cycling in a period of dynamic oxygenation of Earth's surface environments. Our aim is to provide deeper insight and understanding of oceanic oxygenation during a period of climate change and biospheric mass extinction.

2. Background

Research on ocean redox evolution across the O-S boundary indicates a dynamic interval of about 2 Myr, with relatively more anoxic marine waters in the Katian, latest Hirnantian, and Rhuddanian (Bartlett et al., 2018; Hammarlund et al., 2012; Luo et al., 2016; Yan et al., 2012; Zhou et al., 2015). The early- through mid-Hirnantian is thought to be characterized by relatively more oxic conditions, driven by the enhanced circulation of cold, dense, and oxygen-rich polar waters to lower latitudes, resulting in a reduction in the extent of oxygen minimum zones (OMZs) (Luo et al., 2016; Yan et al., 2012). A similar mechanism has been proposed as an explanation for a late Hirnantian ocean anoxic event, whereby global cooling reorganized thermohaline

circulation, decreased deep-ocean ventilation, stimulated primary productivity, and enhanced the extent of OMZs (Bartlett et al., 2018). It is becoming clear that global redox across the O-S boundary was spatially and temporally heterogeneous, and was at times decoupled from global climate (Bartlett et al., 2018; Luo et al., 2016; Melchin et al., 2013).

To develop a better understanding of the relationships, or lack thereof, between global climate, ocean redox, and mass extinctions across the O-S boundary, we focus on the biogeochemical nitrogen cycle. Nitrogen isotopes can shed additional light on ocean redox evolution across the O-S boundary, because they are fractionated during biogeochemical redox transformation. Unlike iron speciation, which is primarily controlled by redox changes near the sediment-water interface (Scholz et al., 2014), the nitrogen cycle is more sensitive to anoxia within the water column and, unlike sulfur, nitrogen does not have a major volcanic or hydrothermal source flux.

Nitrogen isotopic data from O-S sections (Figure 1) in present-day China (Luo et al., 2016), Canada (Melchin et al., 2013), and USA (LaPorte et al., 2009) all record limitation of fixed nitrogen in the paleotropics (~10° N, ~15° N, and ~5° S respectively), spurred by widespread ocean anoxia and high rates of denitrification during the Katian, end-Hirnantian, and Rhuddanian. Denitrification is the biologically mediated reduction of oxidized nitrogen species (NO_3^-, NO_2^-) to N_2 gas through multiple intermediate nitrogen oxide products. During the early and middle Hirnantian, positive $\delta^{15}N$ excursions indicate temporary alleviation from fixed nitrogen limitation in shallow tropical sections, consistent with local availability of nitrate (Luo et al., 2016). Shallow-water sections from high-paleolatitudes (~60° S) in the present-day Czech Republic break from this pattern, showing positive $\delta^{15}N$ values from the Katian through the Hirnantian, suggesting persistent nitrate availability and thus more oxic conditions (Melchin et al., 2013). The emerging spatial-temporal trends in nitrogen cycling from the available data suggest that redox changes across the O-S boundary affected nitrogen bioavailability in tropical shallow-water settings. However, these trends have so far not been extended to the subtropics, which is an important step towards reconstructing global patterns.

In addition to tracking redox perturbations, the nitrogen cycle may have been more directly involved in global climate and the mass extinction event. It has been proposed that changes in the global rate of denitrification in part contributed to the onset and termination of glaciation (Luo et al., 2016), as well as the abundance and distribution of prokaryotic and eukaryotic organisms in the global ocean (Cooper et al., 2012; Melchin et al., 2013; Rohrssen et al., 2013). Nitrous oxide (N_2O) is a by-product of denitrification and a potent greenhouse gas, so decreases in the global denitrification rate caused by glacial eustatic sea-level fall or diminishing oxygen minimum zones could act as a positive cooling feedback by decreasing the N_2O flux to the atmosphere. Also, because denitrification removes bioavailable nitrogen (NO_3^- and NO_2^-) from the ocean, eukaryotic organisms that rely more heavily on the presence of fixed nitrogen in the form of nitrate may become advantaged if global rates of denitrification decrease. If such a feedback between climate, redox, and global rates of denitrification existed, then nitrogen cycling is inherently linked to the carbon cycle and the mass extinctions pulses.

2.1. Geologic setting

Samples were collected from the Upper Hartfell Shale and overlying Lower Birkhill Shale formations of the Moffat Shale Group, located in the Southern Uplands terrain of Scotland

(55°25’47’’ N, 3°16’18’’ W). These formations have only been subjected to prehnite-pumpellyite facies metamorphism (Oliver and Leggett, 1980). The ~11 meter section we sampled spans from the late Katian to the Rhuddanian, and was sampled at ~30 cm resolution. The Upper Hartfell Shale is a massive organic-lean (0.02% - 0.15% total organic carbon; TOC) grey shale with subordinate layers of organic-rich (1% - 2% TOC) graptolitic shale referred to as the *anceps* bands (Armstrong and Coe, 1997). These bands are reminiscent of the Lower Birkhill Shale, which is a laminated organic-rich (1.2% - 2.0% TOC) graptolitic black shale with abundant disseminated and layered pyrite. Carbonate is only present in samples from the Hirnantian part of the Upper Hartfell Shale. Carbonate mineralogy and morphology were investigated using X-ray diffraction (XRD), scanning electron microscopy (SEM), and energy-dispersive X-ray spectroscopy (EDS). The sampled section contains over 20 bentonite beds through both formations ranging from 1 cm to 12 cm in thickness. Seven of these beds were sampled for nitrogen and carbon analyses, and two were sampled for X-ray diffraction analyses. Geochemical similarities between these bentonite horizons and bentonite beds deposited in eastern Baltica have been interpreted as evidence for a common volcanic source that transported ash c. 1200 km from modern-day Scandinavia, which was located on the eastern margin of the Iapetus paleo-ocean (Kiipli et al., 2015). The correlation of these bentonites led Kiipli et al. (2015) to hypothesize that Dob’s Linn was situated near the middle of the Iapetus Ocean. Classic interpretations, however, suggest deposition on the eastern continental margin of Laurentia at 30°S, north of the Iapetus suture, and on the more distal section of the continental slope (Armstrong and Owen, 2002; Cocks and Torsvik, 2002). Whichever paleogeography is more correct, what is certain is that a continental slope depositional environment is consistent with the fine-grained nature of the sedimentary rocks, absence of wave-, tidal- or storm-generated sedimentary structures, scarcity of benthic organisms, and low estimated accumulation rates in the Dob’s Linn section (Armstrong and Coe, 1997; Armstrong and Owen, 2002; Hammarlund et al., 2012). Other than the Vinini Creek section in Nevada, USA, all other O-S sections analyzed for nitrogen isotopes were deposited above the shelf-break, hence Dob’s Linn represents one of the most distal and deeper marine sedimentary packages across the O-S boundary to be analyzed for nitrogen isotopes.

3. Methods

3.1 Sample preparation: bulk and kerogen isolates

Bulk samples and kerogen extractions were prepared using standard methodology (e.g. Koehler et al., 2017; Stüeken, 2013). Outcrop samples were cut into ~ 3 x 3 x 2 cm chips and weathering rinds were shaved off with a diamond tip saw to remove modern contaminants. The chips were then crushed with a steel pestle on a steel plate that were covered with clean aluminum foil between each sample. The resulting smaller chips and coarse powder were transferred to clean glass beakers that had previously been heated at 500°C overnight to remove organic contamination. Each sample was then sonicated in ethanol for 2 minutes, followed by 2N HCl for ~20 seconds to further remove modern contaminants from handling, transportation, and storage. The acid was rinsed from the sample three times with 18MΩ milli-Q water, and samples were covered and left to dry in a ventilated oven at 60°C. Samples were then finely powdered using an aluminum oxide puck mill that was thoroughly cleaned with ethanol, 18MΩ milli-Q water, and pre-combusted silica sand between each sample. Sample powders were stored in baked glass scintillation vials.

Before nitrogen and organic carbon analyses, aliquots of bulk shale and bentonite sample powders were decarbonated using the following method: sample powders were acidified with 6 M HCl at 60°C in three iterations over three days. They were then thoroughly rinsed three times with 18 Ω Milli-Q deionized water to remove the acid, and left to dry in a ventilated oven at 60°C for 48 hours.

Methods for sample kerogen extractions were adapted from Robl and Davis (1993). Depending on organic carbon abundance measurements, 1-4 grams of untreated powder were weighed into 250ml Teflon bottles. 100ml of 50% v/v hydrofluoric acid (HF, reagent grade) were added to sample bottles to react overnight in a shaking water bath at 55°C. The acid was then centrifuged and decanted. Any resulting fluoride precipitates (e.g. CaF_2) were eliminated by treating the samples with 100ml of saturated boric acid (reagent grade) in 50% v/v HF overnight in a shaking water bath at 55°C. The acid was decanted, and samples were rinsed three times with 200ml of 18MΩ milli-Q water. Kerogen was transferred from the Teflon bottles to clean glass scintillation vials, frozen, and then freeze-dried for two days.

3.2 Analytical methods

$\delta^{15}N_{bulk}$, $\delta^{15}N_{kerogen}$, total nitrogen (TN), total organic carbon (TOC), and $\delta^{13}C_{org}$ were measured using a Costech ECS 4010 Elemental Analyzer coupled via a Conflo III to a Thermo Finnigan MAT253 continuous-flow isotope-ratio mass spectrometer. Groups containing a maximum of six samples were bracketed by three in-house standards (calibrated to reference materials USGS40 and USGS41; Qi et al., 2003) that were used to calibrate both abundance and isotope analyses as well as to monitor accuracy within individual runs. They were "GA1" ($\delta^{15}N$ = -4.6‰, $\delta^{13}C$ = -28.3‰), "GA2" ($\delta^{15}N$ = -5.7‰, $\delta^{13}C$ = -13.7‰), and "SA" ($\delta^{15}N$ = 11.3‰, $\delta^{13}C$ = -21.3‰). A fourth in-house rock standard "UW McRae" ($\delta^{15}N$ = 5.6‰, $\delta^{13}C$ = -38.1‰) was used to monitor long-term precision. Average analytical accuracy for $\delta^{15}N_{bulk/kerogen}$ and $\delta^{13}C_{org}$ through all runs was 0.16 ± 0.16‰ and 0.08 ± 0.06‰ respectively, and average analytical precision was 0.11‰ and 0.02‰ respectively. The average standard deviation of sample replicates was 0.11‰ for all $\delta^{15}N$ measurements, and 0.15‰ for all $\delta^{13}C_{org}$ measurements. Atomic ratios of organic carbon to total nitrogen (bulk C/N) and organic nitrogen (organic C/N) were calculated from the measured weight percent and molar masses of C and N.

$\delta^{13}C_{carb}$ and $\delta^{18}O_{carb}$ analyses were performed on untreated sample powders using a Kiel III Carbonate Device coupled to a Delta V Plus Thermo Finnigan Isotope Ratio Mass Spectrometer. The Kiel parameters were set to a phosphoric acid temperature of 80°C, 10 drops of acid for each sample, and a reaction time of 10 minutes in order to digest more recalcitrant carbonates such as siderite. Internal calcite standards "C1" ($\delta^{13}C$ = 2.54, $\delta^{18}O$ = -0.42) and "C2" ($\delta^{13}C$ = -48.99, $\delta^{18}O$ = -16.47) that had been calibrated to international standards NBS19, LSVEC, and NBS18 were used to calibrate $\delta^{13}C_{carb}$ and $\delta^{18}O_{carb}$ values on the VPDB scale. A third quality control standard "CQS2" ($\delta^{13}C$ = -2.15, $\delta^{18}O$ = -15.34) was used to track long term precision. In total, 15 standards were run with 20 samples from Dob's Linn. The average analytical accuracy based on all standards was 0.02 ± 0.02‰ and 0.04 ± 0.03‰ for $\delta^{13}C_{carb}$ and $\delta^{18}O_{carb}$ respectively. The average analytical precision based on the in-house standard CQS2 was 0.02‰ and 0.05‰ for $\delta^{13}C_{carb}$ and $\delta^{18}O_{carb}$ respectively. The average standard deviation of sample replicates was 0.1‰ for all $\delta^{13}C_{carb}$ measurements, and 0.2‰ for all $\delta^{18}O_{carb}$ measurements. Because all the standards are calcite, calcite was the assumed mineralogy when correcting the raw $\delta^{18}O_{carb}$ data for fractionation

during phosphoric acid digestion. Fractionation factors during phosphoric acid digestion of carbonate vary depending on mineralogy (Kim et al., 2007). After analysis of the carbonates revealed dolomite/ankerite as the primary carbonate phase, the $\delta^{18}O_{carb}$ data was corrected using the appropriate fractionation factor (Kim et al., 2015, 2007).

3.3 Percent carbonate

The percent carbonate of our samples was initially calculated gravimetrically (e.g. Koehler et al., 2017; Stüeken, 2013), whereby the weight of the samples before and after the acidification was used to estimate percent carbonate. The resulting values were >10% greater than values measured by the Kiel device, prompting suspicion that the phosphoric acid in the Kiel was not properly digesting recalcitrant carbonate in the Dob's Linn samples.

Because recalcitrant carbonates such as siderite are notoriously hard to digest in phosphoric acid, special attention was given to conditions that will yield complete digestion (e.g. Fernandez et al., 2016). To test if the Kiel III Carbonate Device was completely digesting all carbonates in our samples, we used a methodology similar to Fernandez et al., (2016) "open vessel digestion", which was shown to more rapidly digest siderite. Approximately 50 mg of two Dob's Linn samples were weighed into separate Pyrex reaction tubes. Room-temperature phosphoric acid was added to the reaction tubes but did not interact with the sample at the bottom of the tube because of its high viscosity. Reaction tubes were then attached to a vacuum line to remove the headspace, and subsequently flame-sealed. They were then vortexed to mix the acid with the sample and placed in an oven overnight at 100°C. The tubes were intermittently vortexed during the hot digestion period to ensure the acid was completely mixing with the sample. After the digestion period, the tubes were cracked on a vacuum line and gasses were cryogenically cleaned to isolate the CO_2 produced by the digestion. The amount of CO_2 produced by the digestions was then measured manometrically.

3.4 Quantitative XRD

Four shales and two bentonite samples were prepared for bulk rock analysis by XRD by milling 3 g of sample for 12 minutes in ethanol in a McCrone mill and spray drying the slurry directly from the mill, as described by (Hillier, 1999). The resulting powder specimens were run on a Bruker D8 Advance instrument between 4 and 70° 2θ, using Ni-filtered Cu radiation and counting for 96 seconds in 0.017° steps. Quantitative whole rock mineralogical analyses were made by a prior measured full pattern fitting Reference Intensity Ratio (RIR) approach as detailed for participant #18 in (Omotoso et al., 2006). To enable more detailed clay mineral analysis, <2 µm clay size fractions were separated from the samples by timed sedimentation according to Stokes' law and prepared as oriented specimens mounted on glass by the filter peel transfer method. These specimens were run on a Siemens D5000 using Fe filtered Co radiation, (2-45°2θ, 0.02 steps, 2 seconds per step) air-dried, after ethylene glycol solvation and after heating to 350°C for one hour on a hot plate. Relative proportions of illitic clays (Illite plus mixed-layer illite/smectite) and chlorite were quantified using RIR's calculated with the NEWMOD program according to procedures given in Moore and Reynolds (1997) and Hillier (2003).

4. Results

4.1 Carbonate

Carbonate [%] in bulk shale samples are all below 1% (the limit of detection with our analytical setup) except during the middle Hirnantian where values peak at 23% (Figure 2). This result is confirmed in the XRD data presented in Section 4.3. $\delta^{13}C_{carb}$ and $\delta^{18}O_{carb}$ values for carbonates in Hirnantian shales samples average -4.9 ± 0.4 ‰ and -5.7 ± 0.3 ‰ respectively (Figure 3).

The two Dob's Linn samples that were reacted with phosphoric acid overnight at 100°C and measured manometrically are within 1% of the percent carbonate values produced by Kiel analysis, suggesting that the Kiel carbonate values are reliable. Furthermore, carbonate abundances determined in a few samples by XRD closely match those determined by the Kiel. This means the gravimetrically-determined carbonate abundances were inaccurate (overestimating by more than 10%), likely due to the dissolution of non-carbonate species by the hot concentrated HCl or due to physical loss of material during acid decanting. Regardless, all carbonate values (isotopes and abundances) discussed below refer to the Kiel-measured values.

4.2 Nitrogen and organic carbon

The transition from the Lower Birkhill to the Upper Hartfell coincides with an order-of-magnitude reduction in the abundance of organic carbon from 1.6% ± 0.3% to 0.11% ± 0.11% (Figure 2). The atomic C/N ratios of kerogen extracts are identical (110 ± 12), and the abundances of silicate-bound nitrogen in bulk rock shale samples are invariant (0.05% ± 0.006%), through both formations. Thus, the fraction of nitrogen bound in organic matter ($F_{kerogen}$) rather than in silicates is an order of magnitude greater in Lower Birkhill shales (26.2 ± 3.6%) than in the Upper Hartfell shales (2.8 ± 2.6%) (Appendix 1; Equation 1). In both formations, silicate-bound nitrogen is the dominant nitrogen fraction.

$$F_{kerogen} = 1 - F_{silicate} = \frac{N\ [\%]_{kerogen}}{C\ [\%]_{kerogen}} \times \frac{TOC\ [\%]_{bulk}}{TN\ [\%]_{bulk}} \qquad (1)$$

In bentonite samples TOC [%] values average 0.05% ± 0.02% - comparable to the Upper Hartfell shale - but TN [%] values average 0.163% ± 0.015% and are approximately triple those from shale samples (Figure 2). Because the silicate-bound nitrogen fraction is large and silicate-bound nitrogen abundances are invariant in the Upper Hartfell and bentonite samples, bulk rock C/N ratios are strongly correlated to TOC [%] ($R^2 > 0.94$; Figure 4). This correlation is much weaker in the Lower Birkhill because the variability in organic matter C/N ratios - in this more organic rich formation - contributes more significantly to bulk rock C/N values.

$\delta^{15}N_{bulk}$ values through both the Upper Hartfell Shale and Lower Birkhill Shale are relatively invariant and range from +0.7‰ to -0.1‰ (Figure 5). $\delta^{15}N_{bulk}$ values from the bentonite horizons are equally invariant and on average slightly more negative, ranging from -0.47‰ to -1.25‰. $\delta^{15}N_{kerogen}$ measurements through both formations are more varied, ranging from -6.0‰ to +1.3‰, with seven out of ten samples containing $\delta^{15}N_{kerogen}$ values that are >1‰ depleted in ^{15}N compared to the bulk rock measurement of the same sample (Figure 5).

$\delta^{13}C_{org}$ measurements from the shales agree with those of previous studies (e.g. Finlay et al., 2010; Underwood et al., 1997), with values peaking up to -29.3‰ during the middle Hirnantian, followed by a steady decrease to more depleted values averaging -32.8‰ starting at

the lithological boundary to the Birkhill Shale (Figure 5). One $\delta^{13}C_{org}$ measurement in the late Katian is enriched to a similar magnitude (-29.1‰), also corroborating a prior study (Finlay et al., 2010). Bentonite samples are all enriched in $\delta^{13}C_{org}$ compared to adjacent shale samples, ranging from -26‰ to -30‰ (Figure 6). Differences between kerogen and bulk shale $\delta^{13}C_{org}$ measurements of the same sample are all less than 0.5‰.

4.3 X-ray diffraction

Table 1: X-ray diffraction data for a subset of Dob's Linn shale and bentonite samples.

	Quartz	K-feld	Plag	Calc	Dol	Anatase	Pyrite	Chl (Tri)	Illite+I/S
-9.86m Shale	26.4	0.1	7.9	0	0.1	0	0.2	14.1	51.4
-4.69m Shale	30.3	0.2	7	1.5	14.1	0	0.4	10.6	35.9
-2.51m Shale	38.3	0.3	9.6	0	0	0	0	1.6	50.2
-1.31m Shale	41.7	0.1	8.4	0	0.1	0	7.2	4.1	38.3
+0.8m Bent	6.3	0	3.7	0	0.2	0.9	0.1	0.3	88.5
-8.8m Bent	1.9	0.2	2.1	0	0.1	0.6	0	0	95.1

† *Samples -9.86, -4.69, and -8.8 are from the Upper Hartfell Fm. Samples -2.51, -1.31, and +0.8 are from the Lower Birkhill Fm. Bent – bentonite samples; K-feld – K-feldspar; Plag – plagioclase; Calc – calcite; Dol - dolomite; Chl – chlorite; I/S – illite/smectite mixed-layer.*

The X-ray diffraction results show varying mineralogy through the Dob's Linn section. The one sample analyzed from the Hirnantian glacial period (-4.69) has abundant carbonate phases – mainly dolomite with subordinate calcite – confirming carbonate measurements made by the Kiel (Section 4.1). SEM-EDS images show the primary phase is polymodal, euhedral to subhedral dolomite with subordinate calcite (Figure 7). Bentonite samples are characterized by substantially more illite + illite/smectite (I/S) relative to shale samples. Samples that have relatively more illite + I/S have higher silicate-bound nitrogen concentrations (Figure 8).

5. Discussion

5.1 Potential for post-depositional alteration

5.1.1 Metamorphism

The effects of sub-greenschist metamorphism on $\delta^{15}N$ values is thought to be < 2‰ (Ader et al., 2016; Stüeken et al., 2017) and should therefore be insignificant for our sample set. Classic signs of metamorphic alteration include increasing $\delta^{15}N$ values correlated to increasing C/N ratios, and a divergence between $\delta^{15}N_{silicate}$ and $\delta^{15}N_{kerogen}$ values in a given sample. This is because nitrogen is more mobile than carbon during metamorphism, and ^{14}N is more mobile than ^{15}N under such conditions. There is no correlation between $\delta^{15}N$ and C/N ratios in the Dob's Linn data (Figure 6), however, two samples display $\Delta^{15}N_{silicate\text{-}kerogen}$ values of greater than 4‰. In rocks of low metamorphic grade that have not undergone fluid alteration and migration of ammonium, $\delta^{15}N_{bulk}$ values are usually a good approximation for the original $\delta^{15}N$ values of deposited organic matter (Stüeken et al., 2017). However, the fact that all bentonite horizons are characterized by large TN [%] values, very low C/N ratios, and $\delta^{15}N_{bulk}$ values that closely resemble the $\delta^{15}N_{kerogen}$

from the Lower Birkhill (Figures 2 and 6) suggests that NH_4^+ was likely mobile after sediment deposition and homogenized silicate-bound $\delta^{15}N$ through the section (see below).

There is no correlation between carbonate abundance or $\delta^{13}C_{carb}$ and $\delta^{13}C_{org}$ values, indicating that the $\delta^{13}C_{org}$ excursion in the Dob's Linn section is unlikely to be a result of carbon isotopic equilibration between organic matter and carbonate, which only occurs at higher metamorphic grades above mid-greenschist facies (e.g. Hayes et al., 1983; Hoefs and Frey, 1976; McKirdy and Powell, 1974).

5.1.2 Effects of post-depositional ammonium migration on $\delta^{15}N_{bulk}$

It is likely that $\delta^{15}N_{bulk}$ values through the section, particularly through the more organic-lean Upper Hartfell shale, do not strictly reflect the stratigraphically equivalent $\delta^{15}N$ of original organic matter. TOC is low in the bentonite horizons, as expected during rapid sedimentation rates associated with volcanic ash falls (Figure 2). If silicate-bound nitrogen contained in the bentonites were sourced from associated organic matter, then TN in these bentonite horizons should be correspondingly low. However, TN values (0.16% ± 0.016) are triple and double those seen in Upper Hartfell and Lower Birkhill shales, respectively (Figure 2). These elevated nitrogen levels are most parsimoniously explained by NH_4^+ diffusion through these sediments during illitization (Williams et al., 1992; Williams and Ferrell, 1991), leading to post-depositional enrichment of the bentonites. The bentonite layers likely accumulated relatively more ammonium than the shale samples because the bentonites have proportionally more illitic clay, which has been shown to take up NH_4^+ in substitution for K^+ (Table 1, Figure 8, Schroeder and McLain, 1998). The correlation between silicate-bound nitrogen and illite + I/S abundance points to an invariable clay-normalized silicate-bound nitrogen abundance through all sample types in the section (bentonites and shales), suggesting ammonium concentrations in pore water or migrating fluids was invariable through the section during nitrogen substitution into clay minerals (Williams et al., 1992).

A plausible source for the NH_4^+ is the organic-rich Birkhill Shale, where NH_4^+ was likely mobilized during diagenetic degradation or maturation of organic matter. This process is commonly observed in modern organic-rich sediments where porewaters can reach mM concentrations of NH_4^+ (e.g. Boudreau and Canfield, 1988; Rosenfeld, 1979). Alternatively, NH_4^+ could have been sourced from the overlying water column during bentonite deposition if deep waters were euxinic at the time (Stueken et al., 2016). This is because sulfate reduction, which drives euxinia, cannot be thermodynamically coupled to NH_4^+ oxidation and therefore leads to accumulation of dissolved NH_4^+. However, iron speciation data from Dob's Linn record possible hints of euxinia only in the early Silurian but not during the Ordovician, *i.e.* long after the deposition of the first ash beds (Hammarlund et al. 2012). It is therefore unlikely that the NH_4^+ in the bentonites was directly absorbed from the water column during deposition. It is possible that some of the silicate-bound nitrogen was sourced from ammonium produced by diagenetic biomass degradation *in-situ*, however if this were the case, the low TOC and C/N ratios in the Upper Hartfell would require a diagenetic mechanism that oxidized a lot of carbon without oxidizing nitrogen. Again, microbial sulfate reduction can do this, but then pyrite abundance should be higher than it is in the Upper Hartfell (Hammarlund et al., 2012). Post-depositional migration of NH_4^+ derived from organic-rich sediments is a more likely explanation for most of the silicate-bound nitrogen through the Dob's Linn section. Importantly, the isotopic composition

of the bentonites deviates by less than 1‰ from the surrounding sediments, including the Birkhill Shale, which is most likely the NH_4^+ source rock. This similarity suggests that NH_4^+ mobility and assimilation into secondary illite does not impart a significant isotopic fractionation.

We can estimate the percentage of nitrogen in Upper Hartfell shales that is authigenic rather than derived from the Lower Birkhill Formation (allogenic), if we assume that the Upper Hartfell Formation had a similar average C/N [%] ratio to the Lower Birkhill Formation before diagenetic NH_4^+ migration. This is a fair assumption because the average C/N ratio of kerogen in the Upper Hartfell and Lower Birkhill is identical.

$$TN_{auth.Hartfell} = \frac{TOC_{Hartfell}}{TOC_{Birkhill} \div TN_{Birkhill}} \qquad (2)$$

Here $TN_{auth.Hartfell}$ is the nitrogen percentage of a given shale sample that is estimated to be indigenous in an Upper Hartfell sample, $TOC_{Hartfell}$ is the total organic carbon percentage of the same sample, and $TOC_{Birkhill}$ and $TN_{Birkhill}$ are the average organic carbon percentages and average total nitrogen percentages, respectively, of all Lower Birkhill shale samples. Using the measured total nitrogen percentage of bulk Upper Hartfell samples ($TN_{bulk.Hartfell}$) we can then calculate the fractions of authigenic ($F_{N.auth.Hartfell}$) and allogenic ($F_{N.allo.Hartfell}$) nitrogen:

$$\frac{TN_{auth.Hartfell}}{TN_{bulk.Hartfell}} = F_{N.auth.Hartfell} = 1 - F_{N.allo.Hartfell} \qquad (3)$$

This calculation suggests that 93 ± 3 % of the nitrogen is likely allogenic, derived from the Lower Birkhill Formation. We can explore estimates for the original nitrogen isotopic composition of both these fractions using the following mass balance equation:

$$\delta^{15}N_{auth.Hartfell} = \frac{[\delta^{15}N_{bulk.Hartfell} - (F_{N.allo.Hartfell} * \delta^{15}N_{allo.Hartfell})]}{F_{N.auth.Hartfell}} \qquad (4)$$

Here $\delta^{15}N_{auth.Hartfell}$ and $\delta^{15}N_{allo.Hartfell}$ are the nitrogen isotopic compositions of the original authigenic nitrogen in the Upper Hartfell Formation, and the allogenic nitrogen derived from the Lower Birkhill respectively. $\delta^{15}N_{bulk.Hartfell}$ is the measured bulk nitrogen isotopic value of an Upper Hartfell sample. We assume that the isotopic composition of silicate-bound nitrogen in the lower Birkhill ($\delta^{15}N_{silicate.Birkhill}$) is the best estimate for $\delta^{15}N_{allo.Hartfell}$ because it most likely represents the mobile NH_4^+ in pore fluids that was incorporated into the Lower Birkhill silicates during diagenesis or thermal maturation. Using this assumption in Equation 4, we calculate $\delta^{15}N_{auth.hartfell}$ values that range between -2.5‰ and +1.0‰. Importantly, this range encompasses almost all $\delta^{15}N$ values measured from the Upper Hartfell (bulk and kerogen), and it is broadly similar to the range of values observed in the lower Birkhill Formation, suggesting that authigenic $\delta^{15}N$ was indeed more or less invariant across the whole section prior to NH_4^+ migration.

5.1.3 Diagenesis

Depending on the redox state of the water column and marine sediments, diagenesis can have varying effects on both carbon and nitrogen isotope ratios. In modern marine sediments, residual organic nitrogen can become enriched in ^{15}N as a result of preferential ^{14}N loss during oxic diagenesis (e.g. Altabet and Francois, 2012; Möbius, 2013; Thunell et al., 2004). The magnitude of this enrichment depends on the sediment redox state and sedimentation rates, with greater enrichment (3‰ - 4‰) occurring in oxic sediments with low sedimentation rates. These enrichments approach 0‰ in anoxic sediments and in settings with high sedimentation rates (Robinson et al., 2012).

Depletion of ^{15}N in residual organic nitrogen after diagenesis has been observed in a few modern marine environments (e.g. Fry et al., 1991; Libes and Deuser, 1988), and during laboratory experiments (Lehmann et al., 2002). The mechanism for depletion is thought to be the addition of ^{15}N-depleted biomass through the *in-situ* growth of N_2-fixing bacteria that have an isotopic composition of -2‰ to +1‰. Of course, this would only cause a depletion of ^{15}N in residual organic nitrogen if the organic matter was originally enriched in ^{15}N; *i.e.* biomass dominated by N_2-fixers is unlikely to be isotopically altered by the addition of biomass from more N_2-fixers.

Iron speciation data from Dob's Linn are inconclusive regarding bottom-water redox conditions through this section because they straddle the empirically defined oxic-anoxic boundary (Hammarlund et al., 2012). Further, these data were obtained from outcrop samples hence interpretations must be circumspect in that weathering in outcrop samples can significantly affect sample Fe-S chemistry (Ahm et al., 2017). Without robust independent redox proxies, systematic alteration of $\delta^{15}N$ due to diagenetic redox reactions is difficult to evaluate. This difficulty is compounded by the fact that these strata likely experienced post-depositional ammonium migration (see Section 5.1.2). Assuming our calculations of original Upper Hartfell $\delta^{15}N$ values are correct (Section 5.1.2), then the lack of $\delta^{15}N$ variability through the section suggests that preferential large-scale diagenetic redox effects are unlikely.

Carbonates preserved in the middle Hirnantian beds at Dob's Linn have relatively light $\delta^{13}C_{carb}$ values suggesting that some of the carbonate formed diagenetically from respired biomass. Using average Hirnantian $\delta^{13}C_{carb}$ and $\delta^{13}C_{org}$ values from other coeval sections (0‰ to +5‰ and -28‰ respectively; Melchin et al., 2013) and the average $\delta^{13}C_{carb}$ value from Dob's Linn, mass balance predicts that ~20% to 30% of the carbon in the Dob's Linn carbonates comes from respired organic matter. This, coupled with the dolomite rhombs shown in figure 7, indicates that the carbonate likely formed during early diagenesis rather than syndepositionally. There is no correlation between $\delta^{13}C_{carb}$ and $\delta^{18}O_{carb}$ (Figure 3), and the $\delta^{18}O_{carb}$ values of the Dob's Linn carbonates are within the range of well-preserved subtropical Hirnantian carbonates (-4‰ to -6‰; Armstrong et al., 2009), suggesting limited post-depositional alteration of the original carbonate carbon and oxygen isotopic signals.

5.2 Interpretation of nitrogen isotopes at Dob's Linn

Even after accounting for post-depositional migration of ammonium, almost all nitrogen isotope values (both bulk and kerogen measurements) from the Dob's Linn section fall within the window attributed to biological nitrogen fixation by the Mo-nitrogenase metabolism (-2‰ to +1‰). The predominance of this metabolism suggests that the pool of dissolved ammonium and nitrate was small, because otherwise one would expect large isotopic fractionations of several

per mil imparted by partial assimilation, nitrification, and water column denitrification (Ader et al., 2016). For example, partial denitrification in oxygen minimum zones of the modern nitrate-rich ocean (~30μM) produces isotopically heavy residual nitrate with an isotopic composition of +5‰. This composition is recorded in biomass of nitrate-assimilating organisms (Sigman et al., 2009). Similarly, microbial cultures from ammonium-enriched media (>10μM) show significantly negative isotopic compositions (<-5‰) reflective of partial ammonium uptake from a large reservoir (e.g. Hoch et al., 1992). Hence, the absence of either large positive or negative $\delta^{15}N$ values at Dob's Linn suggests that bioavailable nitrogen, including nitrate and ammonium, may have been persistently limited in this offshore environment across the O-S boundary. In the modern ocean, the signature of biological nitrogen fixation is mainly preserved in anoxic basins like the Black Sea or the Cariaco Basin during interglacial periods (e.g. Fulton et al., 2012; Haug et al., 1998). By analogy, the absence of a significant reservoir of fixed nitrogen across the O-S boundary may reflect relatively anoxic conditions with perhaps low levels of ammonium at depth (reviewed by Stüeken et al., 2016). Although the surface ocean was most likely oxygenated under the oxic Phanerozoic atmosphere, a significant reservoir of nitrate could probably never build up because conversion of NH_4^+ to NO_3^- would have been followed by rapid denitrification at a shallow chemocline, quantitatively converting all NO_3^- to N_2, depleting bioavailable nitrogen and giving nitrogen fixers an ecological advantage (Luo et al., 2016).

5.2.1 Nitrogen cycling across the Ordovician-Silurian Boundary

The nitrogen isotope trend observed across the O-S boundary at Vinini Creek (Nevada, USA), which was deposited in a continental rise to ocean-floor setting but at a tropical latitude (Finney et al., 2007; Finney and Perry, 1991; LaPorte et al., 2009), is very similar to that observed at Dob's Linn. The addition of the Dob's Linn nitrogen data highlights the muted response of offshore and non-tropical settings during the Hirnantian glaciation compared to shallow water tropical settings that saw an alleviation of fixed nitrogen limitation and an increase in steady-state nitrate concentrations across this same period (LaPorte et al., 2009; Luo et al., 2016; Melchin et al., 2013). Though the scarcity of sections measured for nitrogen isotopes across the O-S boundary prohibits confident reconstructions of the global ocean at that time, it appears that within each age (Katian, Hirnantian, and Rhuddanian) there are statistically significant differences in $\delta^{15}N$ values between sections at different latitudes and depositional environments (Table 2; Figure 9 and S1). The highest values tend to be restricted to shallow subpolar waters, and values tend to be slightly elevated in shallow tropical settings during the Hirnantian glaciation.

This spatial pattern is explainable by mechanisms that drive modern oceanic latitudinal trends in nitrogen cycling, though the effects on $\delta^{15}N$ values are inverse compared to the Ordovician. In both instances, cold polar and subpolar waters have higher oxygen solubilities than equatorial and tropical waters. In addition, stronger high-latitude winds drive more vigorous vertical water column mixing (Galbraith et al., 2004). As a consequence, higher oxygen concentrations in these high-latitude waters inhibit or weaken water column denitrification (a reaction requiring suboxic-anoxic waters), resulting in higher nitrate concentrations in polar waters compared to lower latitudes (Altabet and Francois, 1994). Less pervasive oxygenation in the Ordovician (e.g. Bartlett et al., 2018; Hammarlund et al., 2012; Luo et al., 2016; Yan et al., 2012; Zhou et al., 2015) likely resulted in persistent but non-quantitative water column denitrification in polar waters (Melchin et al., 2013), while polar waters in the modern ocean are

more pervasively oxygenated and water column denitrification is limited. This pattern results in a broad latitudinal $\delta^{15}N$ value minimum in modern polar waters (Altabet and Francois, 1994), but seems to have created a $\delta^{15}N$ value maximum in Ordovician polar waters.

These generalizations are subject to spatial/temporal variability as observed in marine sediment cores that span the Pleistocene glacial episodes (Galbraith et al., 2004). During interglacial periods at lower latitudes $\delta^{15}N$ values reflect nitrogen limitation and enhanced denitrification in the Mediterranean and African Margin respectively, resulting from the more sluggish transport of warmer polar waters that contained less dissolved oxygen (Calvert et al., 1992; Galbraith et al., 2004). During glacial periods, limitation of fixed nitrogen was evidently alleviated in the Mediterranean and rates of denitrification reduced along the African Margin, resulting from more efficient transport of cooler oxygen-rich polar water towards the equator (Calvert et al., 1992; Galbraith et al., 2004). It is noteworthy that records from the South China Sea show no glacial-interglacial variability through this same period (Kienast, 2000), so these effects are subject to spatial heterogeneity. However, climatic controls on the transport of oxygen from the poles to the equator, its dynamic effect on oxygen minimum zones and associated denitrification, and the resulting relative abundance of nitrate in the global ocean are well documented from the past 300 kyrs (Galbraith et al., 2004). These physical oceanographic processes and their effects on latitudinal trends in marine nitrogen cycling should have operated through the Phanerozoic, and the data compilation from the O-S boundary may indicate that these processes were operating 444 Myr ago through the Hirnantian glaciation.

The difference between average modern ocean $\delta^{15}N$ values (~5‰) and average Ordovician/Silurian $\delta^{15}N$ values (~1.2‰) indicate that the oceanic nitrate reservoir was overall smaller across the O-S boundary than in the modern ocean, which is consistent with independent evidence of anoxic deep-water conditions (Ahm et al., 2017; e.g. Bartlett et al., 2018; Hammarlund et al., 2012). This redox difference may explain the diametric latitudinal trend in $\delta^{15}N$ values between the Ordovician/Silurian and modern ocean. The mild elevation in $\delta^{15}N$ during the Hirnantian glaciation perhaps points to a deepening of the chemocline and relatively more oxygenated conditions, alleviating the limitation of fixed nitrogen in some shallow water settings. However, as indicated by our data from Dob's Linn, zones of fixed-nitrogen limitation perhaps associated with oxygen minimum zones persisted through the Hirnantian glaciation, suggesting the deep ocean probably did not get ventilated during this glacial period.

Table 2: Table showing average $\delta^{15}N$ values in age and depositional bins.

	Katian	**Hirnantian**	**Rhuddanian**
Shallow Tropics	1.1 ± 0.5‰ (3)	2.0 ± 1.0‰ (3)	1.1 ± 0.5‰ (2)
Deep Tropics	0.2 ± 0.4‰ (2)	0.6 ± 0.3‰ (2)	0.1 ± 0.3‰ (1)
Deep Subtropics	-0.4 ± 2.4‰ (1)	0.1 ± 0.8‰ (1)	-0.1 ± 0.6‰ (1)
Shallow Subpolar	3.0 ± 0.2‰ (2)	3.1 ± 0.4‰ (2)	N/A

† *Standard deviations are 1σ. Data are from this study, Luo et al., (2015), Melchin et al., (2013), and Laporte et al., (2009). Parenthetical numbers represent number of units analyzed in each bin. Deep subtropical data are from this study.*

5.3 Nitrogen in the Paleozoic

To put these findings into a broader context, we compared $\delta^{15}N$ values between the periods of the Paleozoic. We compiled over 2300 measurements from 72 units (Table 3) to further elucidate temporal trends in nitrogen cycling. Results of Shapiro-Wilk tests of normality shows that $\delta^{15}N$ values within each period are not normally distributed. Therefore, and because group variances differ significantly, we perform a Kruskal-Wallis test to test the null hypothesis that the group populations have equal dominance (i.e. when an element is drawn from each group population at random, the largest or smallest element is equally likely to come from each group). The results of this test rejected the null hypothesis of equal dominance, and suggested differences in the $\delta^{15}N$ populations among the different periods. We performed a pairwise Mann-Whitney test as a follow up examination of which periods were significantly different from each other. Both Bonferroni and Banjamini-Hochberg corrections were applied to have a conservative and more relaxed approach in dealing with Type I error, respectively. The results are the same for each correction, and it is also worth noting that an ANOVA test produced identical results. The population of $\delta^{15}N$ values, and so global nitrogen cycling, was similar in the Cambrian, Ordovician, Silurian, and Devonian, but significantly more positive in the Carboniferous and Permian (Figure 10 and S2). This observation is broadly consistent with trends highlighted by Algeo et al. (2014), who attributed the rise in $\delta^{15}N$ values during the Carboniferous and Permian to ensuing icehouse conditions. Nitrogen isotope ratios from the Carboniferous and Permian are also on average significantly higher than those from the Hirnantian glaciation.

Table 3: Binned nitrogen isotope data from the Paleozoic.

Periods	Average $\delta^{15}N$	# of Measurements	# of units
Cambrian	1.5 ± 2.2	608	18
Ordovician – Silurian	1.2 ± 1.4	502	13
*Hirnantian	1.8 ± 1.3	202	8
Devonian	1.2 ± 2.1	454	11
Carboniferous	4.6 ± 2.2	409	11
Permian	4.3 ± 4.0	412	19
Total		**2385**	**72**

† *Statistical methods are given in Section 5.2.2. Compilation data is provided in the supplementary materials.*

It is conceivable that this late Paleozoic rise in $\delta^{15}N$ resulted from a combination of linked redox and climatic factors. Some studies suggest an "oxygenation event" in the atmosphere-ocean system concurrent with the rise of early land plants in the Silurian/Devonian (Dahl et al., 2010; Lenton et al., 2016; Lu et al., 2018). Although this event does not appear to be reflected in the existing nitrogen isotope record, it is possible that rising oxygen levels in the Devonian, paired with global cooling in the Carboniferous, allowed for the build-up of oxic, nitrate-rich waters in the global ocean. Alternatively, nitrogen isotopes may point towards a progressive increase in atmospheric oxygen approaching near-modern values in the Carboniferous and Permian (e.g. Glasspool and Scott, 2010). This atmospheric and oceanic oxygenation could have constituted an important climate feedback, lowering global rates of denitrification and the associate greenhouse gas flux of N_2O to the atmosphere.

5.4 Carbon cycling

Carbonate data from Dob's Linn presented here show no carbonate accumulation in Katian and Rhuddanian sediments, but substantially increased carbonate accumulation (up to ~23%) during the Hirnantian glaciation. Importantly, none of the carbonate preserved in these sediments are detrital and/or bioclasts; the disseminated carbonate indicates early diagenetic formation in sediment pore waters (Figures 7 and S3). The prevalence of diagenetic carbonate is further supported by the moderately negative $\delta^{13}C_{carb}$ values that suggest some contribution of light DIC from respiration of organic matter during diagenesis. Futher, the $\delta^{18}O_{carb}$ values match subtropical seawater $\delta^{18}O$ values from this period (Armstrong et al., 2009).

Does the carbonate enrichment in Hirnantian sediments reflect changes to the carbonate saturation state of seawater or porewaters? Sulfate reduction, especially when coupled with the oxidation of methane, can raise the alkalinity of porewaters and yield porewater carbonate precipitation, though these processes are complex and still debated (e.g. Gallagher et al., 2014; Meister, 2014, 2013; Schrag et al., 2013). Although this process could have aided carbonate precipitation, it is perhaps more likely that the seawater carbonate saturation state above Dob's Linn sediments was instrumental in preserving carbonates during the Hirnantian for the following reasons: (i) Although the $\delta^{13}C_{carb}$ is relatively depleted to around -5‰ suggesting carbon contribution from respired organic matter, the majority of the carbon in these diagenetic carbonates presumably comes from seawater DIC based on isotope mass balance (Section 5.1.3), which means that seawater carbonate saturation state still plays a role in these diagenetically-formed carbonates. (ii) Since there is a lack of evidence for redox changes in the iron, sulfur or nitrogen data (Hammerlund et al. 2012; this study) there would need to be an alternative mechanism explaining why the carbonate enrichment only occurs in Hirnantian strata. Combined, these observations indicates that during the Hirnantian, the water column above Dob's Linn sediments were near or over-saturated with respect to the carbonate mineral phases allowing carbonate to accumulate. This does not appear to be the case in the Katian and Rhuddanian. The trend in carbonate deposition beyond the shelf break at Dob's Linn mirrors trends observed in the Pacific Ocean during glacial-interglacial cycles over the past 300 kyrs.

As originally recognized in the Pacific Ocean (Arrhenius, 1953), it is evident that the marine carbonate compensation depth (CCD; the depth in the water column where carbonate dissolution balances carbonate production) responds to changes in global climate (e.g. Hays et al., 1969; Shackleton and Opdyke, 1977, 1976). Such responses have been extensively documented through the Cenozoic, particularly during the Quaternary where proxies from deep sea sediment cores record changes in carbonate preservation (Karlin et al., 1992; Lee et al., 2000), CO_3^{2-} concentrations (Broecker and Clark, 2001), and carbonate dissolution rates (Lalicata and Lea, 2011; Wang et al., 2016) that correlate to climate proxies. The timing of these correlations is well known: carbonate accumulation in sediments is at a maximum during late glacial periods and early deglaciation (Lalicata and Lea, 2011; Sun et al., 2017). Within these cycles glacial sea-level minimums down to -130 meters relative to the modern level correlate with CCD-deepening of up to 1800 meters (Karlin et al., 1992). The reasons for this trend are thought to be (i) a reduction in continental shelf area during glacial periods, forcing carbonate deposition offshore, (ii) increased alkalinity due to weathering of emergent marine carbonates, and (iii) outgassing of dissolved CO_2 during glaciations, leading to increasing seawater pH and carbonate accumulation (Anderson et al., 2008; Kerr et al., 2017; Yu et al., 2013, 2010). Lowering of the CCD below Dob's

Linn sediments deposited in a continental slope depositional environment hints at the potential magnitude of changes to the global carbonate cycle across the Hirnantian glaciation.

Similar trends in carbonate preservation have been documented in other O-S sections (Figure 11). Both outer- and inner-shelf sections from South China (the Wangjiawan and Nanbazi respectively) show a similar pattern of shale deposition during the Katian and Rhuddanian, and carbonaceous shale/argillaceous limestone deposition during the Hirnantian (Chen et al., 1999; Yan et al., 2009). Deposition at the continental rise to ocean-floor Vinini Creek (USA) section (Finney et al., 2007; Finney and Perry, 1991) is complicated by significant sediment contributions from platform carbonates and silicates. Changes in carbonate abundance at Vinini Creek, often in the form of skeletal fragments and peloids, has been attributed to the relative productivity of a "carbonate factory" on a nearby subtidal platform (Finney et al., 2007; Finney and Perry, 1991; LaPorte et al., 2009). There, the Katian *D. ornatus* zone contains sediments that have up to 90% carbonate by weight (LaPorte et al., 2009), but the subsequent Katian zones leading up to the Hirnantian (*P. pacificus* and *D. mirus*) are notably more carbonate poor, dominated by organic-rich shales with subordinate lime mudstones. Hirnantian sediments at Vinini Creek comprise lime mudstones and thickening limestone beds (Finney et al., 2007; LaPorte et al., 2009). Cessation and resumption of carbonate production has been qualitatively linked to changes in sea level, but it is possible that platform carbonate productivity and export to the Vinini Creek locale was influenced by a fluctuating CCD. The carbonate poor *P. pacificus* and *D. mirus* zones would thus represent a period of CCD shallowing where corrosive bottom waters prohibited allochthonous carbonate accumulation. Any differences between carbonate deposition at Vinini Creek, Dob's Linn, and the two South China sections could reflect paleo-CCD spatial heterogeneity (between the western Panthalassic, Iapetus, and paleo-Tethys Oceans) or perhaps that the periplatform depositional setting at Vinini Creek was unique. Other shallow sections across the O-S seem to have never been below the CCD (e.g. Melchin et al., 2013). This finding supports the importance of deep-sea authigenic carbonate in the global carbon cycle (Schrag et al., 2013; Sun and Turchyn, 2014), particularly before the evolution of planktonic foraminifera and coccolithophores, and extends the relationship observed between deep-sea carbonate cycling and climate in the Pacific Ocean during the Quaternary back to the Ordovician.

6. Conclusions

We demonstrate that nitrogen archives in sedimentary rocks can be affected by diagenetic migration of ammonium, which is derived from organic matter remineralization and trapped in clay minerals, especially illites. However, isotopic fractionations associated with this process are small (<1‰) and can be accounted for in future studies of nitrogen cycling in deep time.

Our data from Dob's Linn, paired with compilations from the literature, yield additional insight on the climate-redox landscape of the late Ordovician-early Silurian ocean. In agreement with previous work, we conclude that the Katian and Rhuddanian are characterized by $\delta^{15}N$ values consistent with fixed nitrogen limitation in most environments except for two subpolar sections. This implies widespread anoxia and high rates of denitrification and is inconsistent with ideas suggesting that widespread ocean oxygenation occurred at this time. Further, despite the overall lower abundance of nitrate in seawater, the spatial trend in $\delta^{15}N$ values hints that – similar

to today – latitudinal temperature gradients in the Paleozoic led to slightly elevated marine nitrate levels in subpolar regions compared to lower latitudes.

An increase in shallow tropical $\delta^{15}N$ values during the Hirnantian is consistent with shrinking oxygen minimum zones and decreasing rates of denitrification, resulting from more efficient transport of colder, oxygen-rich waters from polar regions. Suppressed denitrification and N_2O production could have acted as a positive feedback for climate cooling. However, in the continental slope and rise environments at Dob's Linn (this study) and Vinini Creek, anoxia persisted and ecosystems remained limited in fixed nitrogen.

The CCD in the paleo-Tethys and Iapetus oceans may have been fairly shallow during the Katian and Rhuddianian, potentially above the inner-shelf setting of the Nanbazi section and the deeper Wangjiawan and Dob's Linn settings. An increase in carbonate deposition during the Hirnantian and deepening of the CCD during that glaciation is indicated by the increase in carbonate content at Dob's Linn. We view this relationship between deep-sea carbonate deposition and climate change at the O-S boundary as a deep-time analogue of the Quaternary Pacific-style climatically induced CCD oscillations.

Acknowledgements

This study was funded by University of Washington Department of Earth and Space Sciences Harry Wheeler Scholarship and Jody Bourgeois Graduate Student Support Fund granted to MCK. Stephen Hillier acknowledges support of the Scottish Government's Rural and Environment Science and Analytical Services Division (RESAS). We thank the U.W. Isolab and Andy Schauer for technical support, and Roger Buick for helpful discussions and comments. We also thank Sebastian Fischer and Kärt Üpraus for help in the field. Magali Ader, Linda Kah (reviewers) and Thomas Algeo (editor) are thanked for helpful comments that improved the manuscript.

References

Ader, M., Thomazo, C., Sansjofre, P., Busigny, V., Papineau, D., Laffont, R., Cartigny, P., Halverson, G.P., 2016. Interpretation of the nitrogen isotopic composition of Precambrian sedimentary rocks: Assumptions and perspectives. Chem. Geol. 429, 93–110. https://doi.org/10.1016/j.chemgeo.2016.02.010

Ahm, A.-S.C., Bjerrum, C.J., Hammarlund, E.U., 2017. Disentangling the record of diagenesis, local redox conditions, and global seawater chemistry during the latest Ordovician glaciation. Earth Planet. Sci. Lett. 459, 145–156. https://doi.org/10.1016/j.epsl.2016.09.049

Algeo, T.J., Marenco, P.J., Saltzman, M.R., 2016. Co-evolution of oceans, climate, and the biosphere during the "Ordovician Revolution": A review. Palaeogeogr. Palaeoclimatol. Palaeoecol. 458, 1–11. https://doi.org/10.1016/j.palaeo.2016.05.015

Algeo, T.J., Meyers, P.A., Robinson, R.S., Rowe, H., Jiang, G.Q., 2014. Icehouse–greenhouse variations in marine denitrification. Biogeosciences 11, 1273–1295.

Altabet, M.A., Francois, R., 1994. Sedimentary nitrogen isotopic ratio as a recorder for surface ocean nitrate utilization. Glob. Biogeochem. Cycles 8, 103–116. https://doi.org/10.1029/93GB03396

Anderson, R.F., Fleisher, M.Q., Lao, Y., Winckler, G., 2008. Modern CaCO3 preservation in equatorial Pacific sediments in the context of late-Pleistocene glacial cycles. Mar. Chem., Ocean Biogeochemistry: From GEOSECS to JGOFS and beyond - In celebration of the 65th birthday of Peter G. Brewer 111, 30–46. https://doi.org/10.1016/j.marchem.2007.11.011

Armstrong, H.A., Baldini, J., Challands, T.J., Gröcke, D.R., Owen, A.W., 2009. Response of the Inter-tropical Convergence Zone to Southern Hemisphere cooling during Upper Ordovician glaciation. Palaeogeogr. Palaeoclimatol. Palaeoecol. 284, 227–236. https://doi.org/10.1016/j.palaeo.2009.10.001

Armstrong, H.A., Coe, A.L., 1997. Deep-sea sediments record the geophysiology of the late Ordovician glaciation. J. Geol. Soc. 154, 929–934. https://doi.org/10.1144/gsjgs.154.6.0929

Armstrong, H.A., Owen, A.W., 2002. Euconodont paleobiogeography and the closure of the Iapetus Ocean. Geology 30, 1091–1094. https://doi.org/10.1130/0091-7613(2002)030<1091:EPATCO>2.0.CO;2

Arrhenius, G., 1953. Sediment Cores from the East Pacific. Geol. Fören. Stockh. Förh. 75, 115–118. https://doi.org/10.1080/11035895309454862

Bartlett, R., Elrick, M., Wheeley, J.R., Polyak, V., Desrochers, A., Asmerom, Y., 2018. Abrupt global-ocean anoxia during the Late Ordovician–early Silurian detected using uranium isotopes of marine carbonates. Proc. Natl. Acad. Sci. 201802438. https://doi.org/10.1073/pnas.1802438115

Bergström, S.M., Chen, X., Gutiérrez-Marco, J.C., Dronov, A., 2009. The new chronostratigraphic classification of the Ordovician System and its relations to major regional series and stages and to δ13C chemostratigraphy. Lethaia 42, 97–107. https://doi.org/10.1111/j.1502-3931.2008.00136.x

Boudreau, B.P., Canfield, D.E., 1988. A provisional diagenetic model for pH in anoxic porewaters: Application to the FOAM Site [WWW Document]. https://doi.org/info:doi/10.1357/002224088785113603

Broecker, W.S., Clark, E., 2001. Glacial-to-Holocene Redistribution of Carbonate Ion in the Deep Sea. Science 294, 2152–2155. https://doi.org/10.1126/science.1064171

Calvert, S.E., Nielsen, B., Fontugne, M.R., 1992. Evidence from nitrogen isotope ratios for enhanced productivity during formation of eastern Mediterranean sapropels. Nature 359, 223. https://doi.org/10.1038/359223a0

Chen, X., Jia-yu, R., Mitchell, C.E., Harper, D.A.T., Fan, J., Zhang, Y., Zhan, R., Wang, Z., Wang, Y., 1999. Stratigraphy of the Hirnantian substage from Wangjiawan, Yichang, W. Hubei and Honghuayuan, Tongzi, N. Guizhou, China. Acta Univ. Carol. Geol. 233–236.

Cocks, L.R.M., Torsvik, T.H., 2002. Earth geography from 500 to 400 million years ago: a faunal and palaeomagnetic review. J. Geol. Soc. 159, 631–644. https://doi.org/10.1144/0016-764901-118

Cooper, R.A., Rigby, S., Loydell, D.K., Bates, D.E.B., 2012. Palaeoecology of the Graptoloidea. Earth-Sci. Rev. 112, 23–41. https://doi.org/10.1016/j.earscirev.2012.01.001

Dahl, T.W., Hammarlund, E.U., Anbar, A.D., Bond, D.P.G., Gill, B.C., Gordon, G.W., Knoll, A.H., Nielsen, A.T., Schovsbo, N.H., Canfield, D.E., 2010. Devonian rise in atmospheric oxygen

correlated to the radiations of terrestrial plants and large predatory fish. Proc. Natl. Acad. Sci. 107, 17911–17915. https://doi.org/10.1073/pnas.1011287107
Ernst, R.E., Youbi, N., 2017. How Large Igneous Provinces affect global climate, sometimes cause mass extinctions, and represent natural markers in the geological record. Palaeogeogr. Palaeoclimatol. Palaeoecol. 478, 30–52.
Fan, J., Peng, P., Melchin, M.J., 2009. Carbon isotopes and event stratigraphy near the Ordovician–Silurian boundary, Yichang, South China. Palaeogeogr. Palaeoclimatol. Palaeoecol. 276, 160–169. https://doi.org/10.1016/j.palaeo.2009.03.007
Fernandez, A., van Dijk, J., A. Müller, I., M. Bernasconi, S., 2016. Siderite acid fractionation factors for sealed and open vessel digestions at 70 °C and 100 °C. Chem. Geol. 444. https://doi.org/10.1016/j.chemgeo.2016.10.015
Finlay, A.J., Selby, D., Gröcke, D.R., 2010. Tracking the Hirnantian glaciation using Os isotopes. Earth Planet. Sci. Lett. 293, 339–348.
Finnegan, S., Bergmann, K., Eiler, J.M., Jones, D.S., Fike, D.A., Eisenman, I., Hughes, N.C., Tripati, A.K., Fischer, W.W., 2011. The Magnitude and Duration of Late Ordovician-Early Silurian Glaciation. Science 331, 903–906. https://doi.org/10.1126/science.1200803
Finney, S., Berry William B. N., Cooper John D., 2007. The influence of denitrifying seawater on graptolite extinction and diversification during the Hirnantian (latest Ordovician) mass extinction event. Lethaia 40, 281–291. https://doi.org/10.1111/j.1502-3931.2007.00027.x
Finney, S.C., Perry, B.D., 1991. Depositional Setting and Paleogeography of Ordovician Vinini Formation, Central Nevada. JD Cooper CH Stevens Eds Paleoz. Paleogeography West. U. S. II, Society of Economic Paleontologists and Mineralogists Pacific Section, Los Angeles 747–766.
Fry, B., Jannasch, H., Molyneaux, S., Wirsen, C., Muramoto, J., King, S., 1991. Stable Isotope Studies of the Carbon, Nitrogen and Sulfur Cycles in the Black-Sea and the Cariaco Trench. Deep-Sea Res. Part -Oceanogr. Res. Pap. 38, S1003–S1019. https://doi.org/10.1016/S0198-0149(10)80021-4
Fulton, J.M., Arthur, M.A., Freeman, K.H., 2012. Black Sea nitrogen cycling and the preservation of phytoplankton delta N-15 signals during the Holocene. Glob. Biogeochem. Cycles 26, GB2030. https://doi.org/10.1029/2011GB004196
Galbraith, E.D., Kienast, M., Pedersen, T.F., Calvert, S.E., 2004. Glacial-interglacial modulation of the marine nitrogen cycle by high-latitude O2 supply to the global thermocline. Paleoceanography 19. https://doi.org/10.1029/2003PA001000
Gallagher, K.L., Dupraz, C., Visscher, P.T., 2014. Two opposing effects of sulfate reduction on carbonate precipitation in normal marine, hypersaline, and alkaline environments: COMMENT. Geology 42, e313–e314.
Gibbs, M.T., Barron, E.J., Kump, L.R., 1997. An atmospheric pCO2 threshold for glaciation in the Late Ordovician. Geology 25, 447. https://doi.org/10.1130/0091-7613(1997)025<0447:AAPCTF>2.3.CO;2
Glasspool, I.J., Scott, A.C., 2010. Phanerozoic concentrations of atmospheric oxygen reconstructed from sedimentary charcoal. Nat. Geosci. 3, 627–630. https://doi.org/10.1038/ngeo923

Hammarlund, E.U., Dahl, T.W., Harper, D.A.T., Bond, D.P.G., Nielsen, A.T., Bjerrum, C.J., Schovsbo, N.H., Schönlaub, H.P., Zalasiewicz, J.A., Canfield, D.E., 2012. A sulfidic driver for the end-Ordovician mass extinction. Earth Planet. Sci. Lett. 331–332, 128–139. https://doi.org/10.1016/j.epsl.2012.02.024

Haug, G.H., Pedersen, T.F., Sigman, D.M., Calvert, S.E., Nielsen, B., Peterson, L.C., 1998. Glacial/interglacial variations in production and nitrogen fixation in the Cariaco Basin during the last 580 kyr. Paleoceanography 13, 427–432. https://doi.org/10.1029/98PA01976

Hayes, J., W. Wedeking, K., R. Kaplan, I., 1983. Precambrian organic geochemistry - Preservation of the record.

Hays, J.D., Saito, T., Opdyke, N.D., Burckle, L.H., 1969. Pliocene-Pleistocene Sediments of the Equatorial Pacific: Their Paleomagnetic, Biostratigraphic, and Climatic Record. GSA Bull. 80, 1481–1514. https://doi.org/10.1130/0016-7606(1969)80[1481:PSOTEP]2.0.CO;2

Herrmann, A.D., Patzkowsky, M.E., Pollard, D., 2004. The impact of paleogeography, pCO2, poleward ocean heat transport and sea level change on global cooling during the Late Ordovician. Palaeogeogr. Palaeoclimatol. Palaeoecol. 206, 59–74. https://doi.org/10.1016/j.palaeo.2003.12.019

Hillier, S., 2003. Quantitative analysis of clay and other minerals in sandstones by X-ray powder diffraction (XRPD), in: Clay Mineral Cements in Sandstone, Int. Assoc. Sedimetol. Spec. Publ. pp. 213–251.

Hillier, S., 1999. Use of an air brush to spray dry samples for X-ray powder diffraction. Clay Miner. 34, 127–135. https://doi.org/10.1180/000985599545984

Hoch, M., Fogel, M., Kirchman, D., 1992. Isotope Fractionation Associated with Ammonium Uptake by a Marine Bacterium. Limnol. Oceanogr. 37, 1447–1459. https://doi.org/10.4319/lo.1992.37.7.1447

Hoefs, J., Frey, M., 1976. The isotopic composition of carbonaceous matter in a metamorphic profile from the Swiss Alps. Geochim. Cosmochim. Acta 40, 945–951. https://doi.org/10.1016/0016-7037(76)90143-5

Jablonski, D., 1991. Extinctions: A Paleontological Perspective. Science 253, 754–757.

Kah, L.C., Thompson, C.K., Henderson, M.A., Zhan, R., 2016. Behavior of marine sulfur in the Ordovician. Palaeogeogr. Palaeoclimatol. Palaeoecol. 458, 133–153. https://doi.org/10.1016/j.palaeo.2015.12.028

Karlin, R., Lyle, M., Zahn, R., 1992. Carbonate Variations in the Northeast Pacific during the Late Quaternary. Paleoceanography 7, 43–61. https://doi.org/10.1029/91PA03077

Kenrick, P., Wellman, C.H., Schneider, H., Edgecombe, G.D., 2012. A timeline for terrestrialization: consequences for the carbon cycle in the Palaeozoic. Philos. Trans. R. Soc. B Biol. Sci. 367, 519–536. https://doi.org/10.1098/rstb.2011.0271

Kerr, J., Rickaby, R., Yu, J., Elderfield, H., Sadekov, A.Yu., 2017. The effect of ocean alkalinity and carbon transfer on deep-sea carbonate ion concentration during the past five glacial cycles. Earth Planet. Sci. Lett. 471, 42–53. https://doi.org/10.1016/j.epsl.2017.04.042

Kienast, M., 2000. Unchanged nitrogen isotopic composition of organic matter in the South China Sea during the last climatic cycle: Global implications. Paleoceanography 15, 244–253. https://doi.org/10.1029/1999PA000407

Kiipli, T., Dahlqvist, P., Kallaste, T., Kiipli, E., NõLvak, J., 2015. Upper Katian (Ordovician) bentonites in the East Baltic, Scandinavia and Scotland: geochemical correlation and volcanic source interpretation. Geol. Mag. 152, 589–602. https://doi.org/10.1017/S001675681400051X

Kim, S.-T., Coplen, T.B., Horita, J., 2015. Normalization of stable isotope data for carbonate minerals: Implementation of IUPAC guidelines. Geochim. Cosmochim. Acta 158, 276–289. https://doi.org/10.1016/j.gca.2015.02.011

Kim, S.-T., Mucci, A., Taylor, B.E., 2007. Phosphoric acid fractionation factors for calcite and aragonite between 25 and 75 °C: Revisited. Chem. Geol. 246, 135–146. https://doi.org/10.1016/j.chemgeo.2007.08.005

Koehler, M.C., Stueeken, E.E., Kipp, M.A., Buick, R., Knoll, A.H., 2017. Spatial and temporal trends in Precambrian nitrogen cycling: A Mesoproterozoic offshore nitrate minimum. Geochim. Cosmochim. Acta 198, 315–337. https://doi.org/10.1016/j.gca.2016.10.050

Krause, A.J., Mills, B.J.W., Zhang, S., Planavsky, N.J., Lenton, T.M., Poulton, S.W., 2018. Stepwise oxygenation of the Paleozoic atmosphere. Nat. Commun. 9, 4081. https://doi.org/10.1038/s41467-018-06383-y

Lalicata, J.J., Lea, D.W., 2011. Pleistocene carbonate dissolution fluctuations in the eastern equatorial Pacific on glacial timescales: Evidence from ODP Hole 1241. Mar. Micropaleontol. 79, 41–51. https://doi.org/10.1016/j.marmicro.2011.01.002

LaPorte, D.F., Holmden, C., Patterson, W.P., Loxton, J.D., Melchin, M.J., Mitchell, C.E., Finney, S.C., Sheets, H.D., 2009. Local and global perspectives on carbon and nitrogen cycling during the Hirnantian glaciation. Palaeogeogr. Palaeoclimatol. Palaeoecol. 276, 182–195. https://doi.org/10.1016/j.palaeo.2009.03.009

Lee, G.H., Park, S.C., Kim, D.C., 2000. Fluctuations of the calcite compensation depth (CCD) in the East Sea (Sea of Japan). Geo-Mar. Lett. 20, 20–26. https://doi.org/10.1007/s003670000029

Lehmann, M.F., Bernasconi, S.M., Barbieri, A., McKenzie, J.A., 2002. Preservation of organic matter and alteration of its carbon and nitrogen isotope composition during simulated and in situ early sedimentary diagenesis. Geochim. Cosmochim. Acta 66, 3573–3584.

Lenton, T.M., Dahl, T.W., Daines, S.J., Mills, B.J.W., Ozaki, K., Saltzman, M.R., Porada, P., 2016. Earliest land plants created modern levels of atmospheric oxygen. Proc. Natl. Acad. Sci. 113, 9704–9709. https://doi.org/10.1073/pnas.1604787113

Libes, S., Deuser, W., 1988. The Isotope Geochemistry of Particulate Nitrogen in the Peru Upwelling Area and the Gulf of Maine. Deep-Sea Res. Part -Oceanogr. Res. Pap. 35, 517–533. https://doi.org/10.1016/0198-0149(88)90129-X

Lu, W., Ridgwell, A., Thomas, E., Hardisty, D.S., Luo, G., Algeo, T.J., Saltzman, M.R., Gill, B.C., Shen, Y., Ling, H.-F., Edwards, C.T., Whalen, M.T., Zhou, X., Gutchess, K.M., Jin, L., Rickaby, R.E.M., Jenkyns, H.C., Lyons, T.W., Lenton, T.M., Kump, L.R., Lu, Z., 2018. Late inception of a resiliently oxygenated upper ocean. Science 361, 174–177. https://doi.org/10.1126/science.aar5372

Luo, G., Algeo, T.J., Zhan, R., Yan, D., Huang, J., Liu, J., Xie, S., 2016. Perturbation of the marine nitrogen cycle during the Late Ordovician glaciation and mass extinction. Palaeogeogr. Palaeoclimatol. Palaeoecol. 448, 339–348. https://doi.org/10.1016/j.palaeo.2015.07.018

Marenco, P.J., Martin, K.R., Marenco, K.N., Barber, D.C., 2016. Increasing global ocean oxygenation and the Ordovician Radiation: Insights from Th/U of carbonates from the Ordovician of western Utah. Palaeogeogr. Palaeoclimatol. Palaeoecol., The Ordovician Revolution: Co-Evolution of Climate and the Biosphere 458, 77–84. https://doi.org/10.1016/j.palaeo.2016.05.014

McKirdy, D.M., Powell, T.G., 1974. Metamorphic Alteration of Carbon Isotopic Composition in Ancient Sedimentary Organic Matter: New Evidence from Australia and South Africa. Geology 2, 591–595. https://doi.org/10.1130/0091-7613(1974)2<591:MAOCIC>2.0.CO;2

Meister, P., 2014. Two opposing effects of sulfate reduction on carbonate precipitation in normal marine, hypersaline, and alkaline environments: Reply. Geology 42, e315–e315.

Meister, P., 2013. Two opposing effects of sulfate reduction on carbonate precipitation in normal marine, hypersaline, and alkaline environments. Geology 41, 499–502.

Melchin, M.J., Holmden, C., 2006. Carbon isotope chemostratigraphy in Arctic Canada: Sea-level forcing of carbonate platform weathering and implications for Hirnantian global correlation. Palaeogeogr. Palaeoclimatol. Palaeoecol. 234, 186–200. https://doi.org/10.1016/j.palaeo.2005.10.009

Melchin, M.J., Mitchell, C.E., Holmden, C., Štorch, P., 2013. Environmental changes in the Late Ordovician–early Silurian: Review and new insights from black shales and nitrogen isotopes. GSA Bull. 125, 1635–1670.

Möbius, J., 2013. Isotope fractionation during nitrogen remineralization (ammonification): Implications for nitrogen isotope biogeochemistry. Geochim. Cosmochim. Acta 105, 422–432. https://doi.org/10.1016/j.gca.2012.11.048

Moore, D.M., Reynolds, R.C., 1997. X-ray diffraction and the identification and analysis of clay minerals, 2nd ed. Oxford University Press, Oxford.

Nardin, E., Goddéris, Y., Donnadieu, Y., Hir, G.L., Blakey, R.C., Pucéat, E., Aretz, M., 2011. Modeling the early Paleozoic long-term climatic trend. GSA Bull. 123, 1181–1192. https://doi.org/10.1130/B30364.1

Oliver, G.J.H., Leggett, J.K., 1980. Metamorphism in an accretionary prism: prehnite-pumpellyite facies metamorphism of the Southern Uplands of Scotland. Earth Environ. Sci. Trans. R. Soc. Edinb. 71, 235–246.

Omotoso, O., McCarty, D.K., Hillier, S., Kleeberg, R., 2006. SOME SUCCESSFUL APPROACHES TO QUANTITATIVE MINERAL ANALYSIS AS REVEALED BY THE 3RD REYNOLDS CUP CONTEST. Clays Clay Miner. 54, 748–760. https://doi.org/10.1346/CCMN.2006.0540609

Qi, H., Coplen, T.B., Geilmann, H., Brand, W.A., Böhlke, J.K., 2003. Two new organic reference materials for δ13C and δ15N measurements and a new value for the δ13C of NBS 22 oil. Rapid Commun. Mass Spectrom. 17, 2483–2487.

Robinson, R.S., Kienast, M., Albuquerque, A.L., Altabet, M., Contreras, S., Holz, R.D.P., Dubois, N., Francois, R., Galbraith, E., Hsu, T.-C., Ivanochko, T., Jaccard, S., Kao, S.-J., Kiefer, T., Kienast, S., Lehmann, M., Martinez, P., McCarthy, M., Möbius, J., Pedersen, T., Quan, T.M., Ryabenko, E., Schmittner, A., Schneider, R., Schneider-Mor, A., Shigemitsu, M., Sinclair, D., Somes, C., Studer, A., Thunell, R., Yang, J.-Y., 2012. A review of nitrogen isotopic alteration in marine sediments. Paleoceanography 27. https://doi.org/10.1029/2012PA002321

Robl, T.L., Davis, B.H., 1993. Comparison of the HF-HCl and HF-BF3 maceration techniques and the chemistry of resultant organic concentrates. Org. Geochem. 20, 249–255.
Rohrssen, M., Love, G.D., Fischer, W., Finnegan, S., Fike, D.A., 2013. Lipid biomarkers record fundamental changes in the microbial community structure of tropical seas during the Late Ordovician Hirnantian glaciation. Geology 41, 127–130. https://doi.org/10.1130/G33671.1
Rosenfeld, J.K., 1979. Ammonium adsorption in nearshore anoxic sediments. Limnol. Oceanogr. 24, 356–364. https://doi.org/10.4319/lo.1979.24.2.0356
Scholz, F., Severmann, S., McManus, J., Hensen, C., 2014. Beyond the Black Sea paradigm: The sedimentary fingerprint of an open-marine iron shuttle. Geochim. Cosmochim. Acta 127, 368–380. https://doi.org/10.1016/j.gca.2013.11.041
Schrag, D.P., Higgins, J.A., Macdonald, F.A., Johnston, D.T., 2013. Authigenic Carbonate and the History of the Global Carbon Cycle. Science 339, 540–543. https://doi.org/10.1126/science.1229578
Schroeder, P.A., McLain, A.A., 1998. Illite-smectites and the influence of burial diagenesis on the geochemical cycling of nitrogen. Clay Miner. 33, 539–546.
Shackleton, N.J., Opdyke, N.D., 1977. Oxygen isotope and palaeomagnetic evidence for early Northern Hemisphere glaciation. Nature 270, 216–219. https://doi.org/10.1038/270216a0
Shackleton, N.J., Opdyke, N.D., 1976. Oxygen-Isotope and Paleomagnetic Stratigraphy of Pacific Core V28-239 Late Pliocene to Latest Pleistocene [WWW Document]. EPIC3Bremerhaven GSA. URL http://epic.awi.de/35544/ (accessed 5.16.18).
Sigman, D.M., Karsh, K.L., Casciotti, K.L., 2009. Nitrogen Isotopes in the Ocean, in: Steele, J.H. (Ed.), Encyclopedia of Ocean Sciences (Second Edition). Academic Press, Oxford, pp. 40–54. https://doi.org/10.1016/B978-012374473-9.00632-9
Stüeken, E.E., 2013. A test of the nitrogen-limitation hypothesis for retarded eukaryote radiation: Nitrogen isotopes across a Mesoproterozoic basinal profile. Geochim. Cosmochim. Acta 120, 121–139. https://doi.org/10.1016/j.gca.2013.06.002
Stueken, E.E., Kipp, M.A., Koehler, M.C., Buick, R., 2016. The evolution of Earth's biogeochemical nitrogen cycle. Earth-Sci. Rev. 160, 220–239. https://doi.org/10.1016/j.earscirev.2016.07.007
Stueken, E.E., Zaloumis, J., Meixnerova, J., Buick, R., 2017. Differential metamorphic effects on nitrogen isotopes in kerogen extracts and bulk rocks. Geochim. Cosmochim. Acta 217, 80–94. https://doi.org/10.1016/j.gca.2017.08.019
Sun, H., Li, T., Chang, F., Wan, S., Xiong, Z., An, B., Sun, R., 2017. Deep-sea carbonate preservation in the western Philippine Sea over the past 1Ma. Quat. Int., Marine Geology in Asian Marginal Seas: ICAMG-8 459, 101–115. https://doi.org/10.1016/j.quaint.2017.08.041
Sun, X., Turchyn, A.V., 2014. Significant contribution of authigenic carbonate to marine carbon burial. Nat. Geosci. 7, 201–204. https://doi.org/10.1038/ngeo2070
Thunell, R.C., Sigman, D.M., Muller-Karger, F.E., Astor, Y., Varela, R., 2004. Nitrogen isotope dynamics of the Cariaco Basin, Venezuela. Glob. Biogeochem. Cycles 18. https://doi.org/10.1029/2003GB002185

Trotter, J.A., Williams, I.S., Barnes, C.R., Lécuyer, C., Nicoll, R.S., 2008. Did Cooling Oceans Trigger Ordovician Biodiversification? Evidence from Conodont Thermometry. Science 321, 550–554. https://doi.org/10.1126/science.1155814

Underwood, C.J., Crowley, S.F., Marshall, J.D., Brenchley, P.J., 1997. High-Resolution carbon isotope stratigraphy of the basal Silurian Stratotype (Dob's Linn, Scotland) and its global correlation. J. Geol. Soc. 154, 709–718. https://doi.org/10.1144/gsjgs.154.4.0709

Wang, N., Huang, B.-Q., Li, H., 2016. Deep-water carbonate dissolution in the northern South China Sea during Marine Isotope Stage 3. J. Palaeogeogr. 5, 100–107. https://doi.org/10.1016/j.jop.2015.11.004

Williams, L., Ferrell, R., 1991. Ammonium Substitution in Illite During Maturation of Organic-Matter. Clays Clay Miner. 39, 400–408. https://doi.org/10.1346/CCMN.1991.0390409

Williams, L., Wilcoxon, B., Ferrell, R., Sassen, R., 1992. Diagenesis of Ammonium During Hydrocarbon Maturation and Migration, Wilcox-Group, Louisiana, Usa. Appl. Geochem. 7, 123–134. https://doi.org/10.1016/0883-2927(92)90031-W

Yan, D., Chen, D., Wang, Q., Wang, J., 2012. Predominance of stratified anoxic Yangtze Sea interrupted by short-term oxygenation during the Ordo-Silurian transition. Chem. Geol. 291, 69–78. https://doi.org/10.1016/j.chemgeo.2011.09.015

Yan, D., Chen, D., Wang, Q., Wang, J., Wang, Z., 2009. Carbon and sulfur isotopic anomalies across the Ordovician–Silurian boundary on the Yangtze Platform, South China. Palaeogeogr. Palaeoclimatol. Palaeoecol. 274, 32–39. https://doi.org/10.1016/j.palaeo.2008.12.016

Young, S.A., Saltzman, M.R., Foland, K.A., Linder, J.S., Kump, L.R., 2009. A major drop in seawater 87Sr/86Sr during the Middle Ordovician (Darriwilian): Links to volcanism and climate? Geology 37, 951–954. https://doi.org/10.1130/G30152A.1

Yu, J., Anderson, R.F., Jin, Z., Rae, J.W.B., Opdyke, B.N., Eggins, S.M., 2013. Responses of the deep ocean carbonate system to carbon reorganization during the Last Glacial–interglacial cycle. Quat. Sci. Rev. 76, 39–52. https://doi.org/10.1016/j.quascirev.2013.06.020

Yu, J., Broecker, W.S., Elderfield, H., Jin, Z., McManus, J., Zhang, F., 2010. Loss of Carbon from the Deep Sea Since the Last Glacial Maximum. Science 330, 1084–1087. https://doi.org/10.1126/science.1193221

Zhou, L., Algeo, T.J., Shen, J., Hu, Z., Gong, H., Xie, S., Huang, J., Gao, S., 2015. Changes in marine productivity and redox conditions during the Late Ordovician Hirnantian glaciation. Palaeogeogr. Palaeoclimatol. Palaeoecol. 420, 223–234. https://doi.org/10.1016/j.palaeo.2014.12.012

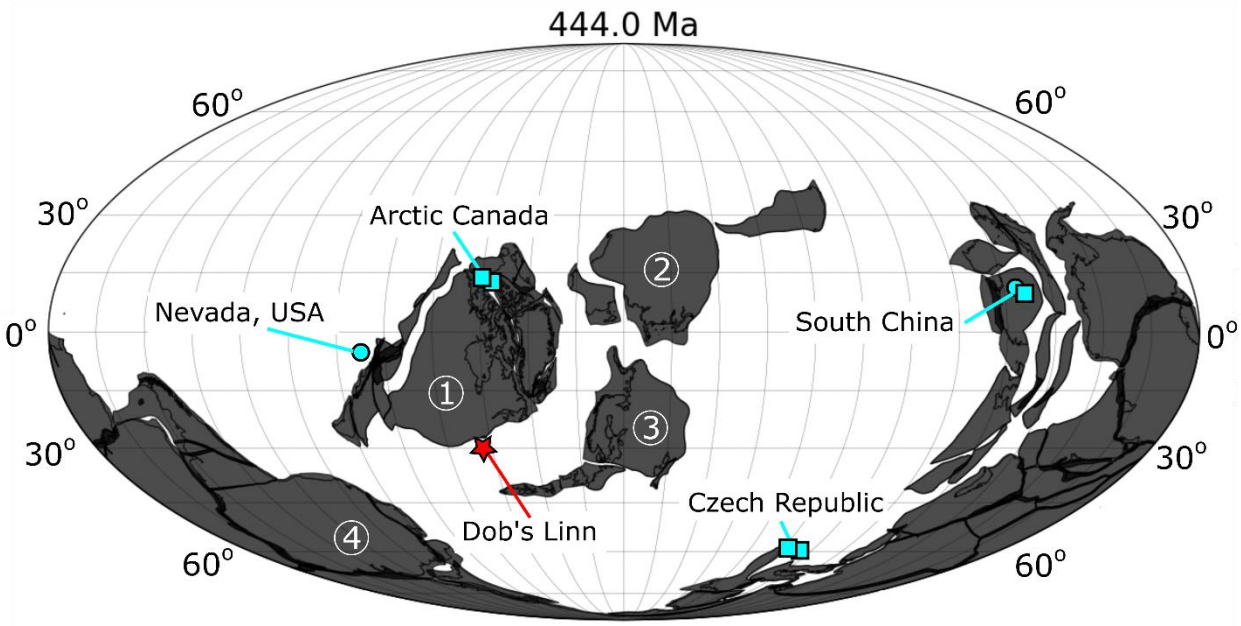

Figure 1: Paleogeographic reconstruction of the Hirnantian using gplates PALEOMAP model. Black represents continental masses, including flooded margins. Red star marks the location of Dob's Linn. Blue circles mark relatively deep sections discussed in the main text that have been analyzed for nitrogen isotopes across the O-S boundary, and blue squares mark relatively shallow sections (LaPorte et al., 2009; Luo et al., 2016; Melchin et al., 2013). Continental land masses are numbered as follows: (1) Laurentia, (2) Siberia, (3) Baltica, (4) Gondwana.

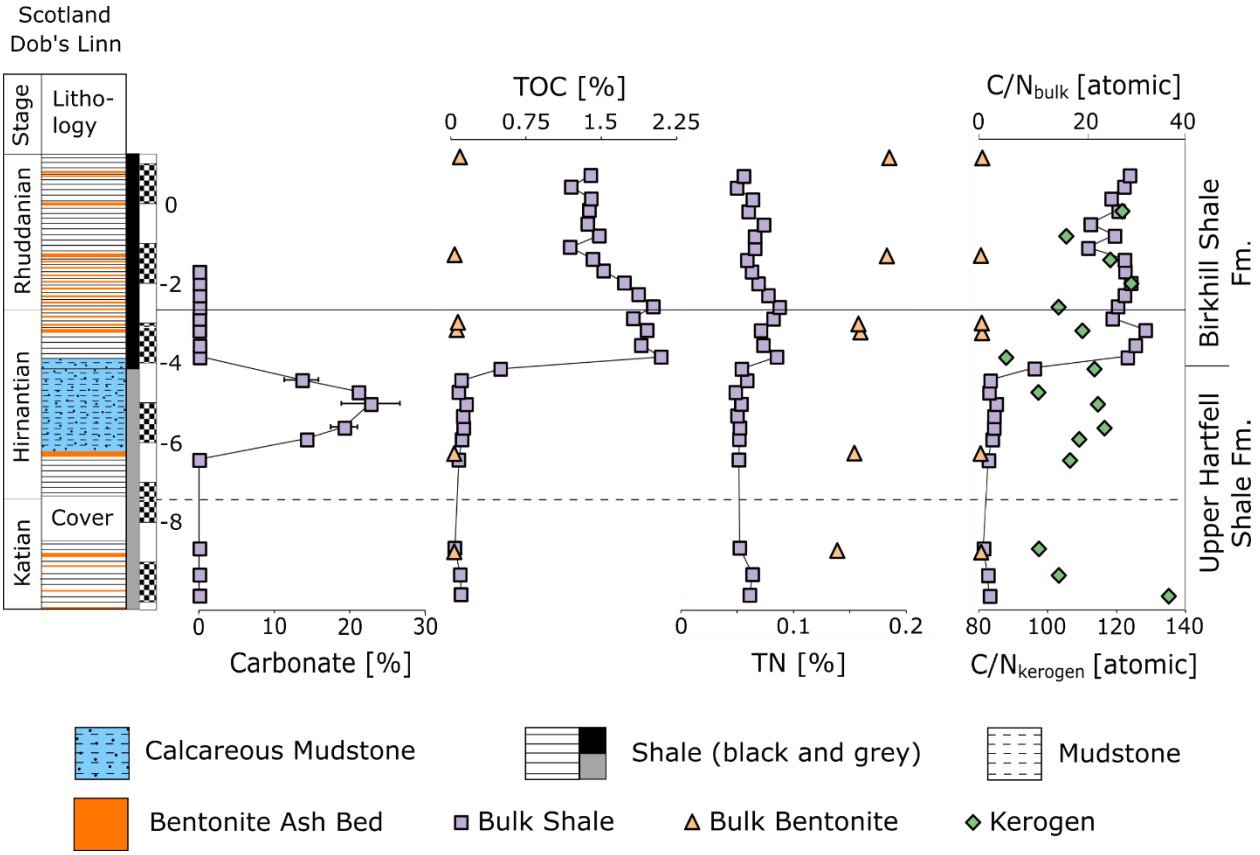

Figure 2: Carbonate abundance, total organic carbon (TOC), total nitrogen (TN), and C/N ratios through the Dob's Linn section. Carbonate is only found in Hirnantian sediments, consistent with a deepening of the CCD during the Hirnantian glacial period. Low TOC but high TN in bentonite samples suggest post-depositional acquisition of ammonium, consistent with ammonium migration through the section during illitization. Kerogen C/N ratios are similar between the Upper Hartfell and Lower Birkhill Formations, suggesting the change in bulk C/N ratios through the section is a function of TOC and silicate-bound nitrogen. Notice the different axes for bulk and kerogen C/N ratios. Bulk measurements are performed on decarbonated sample powders. Kerogen measurements are performed on kerogen isolates.

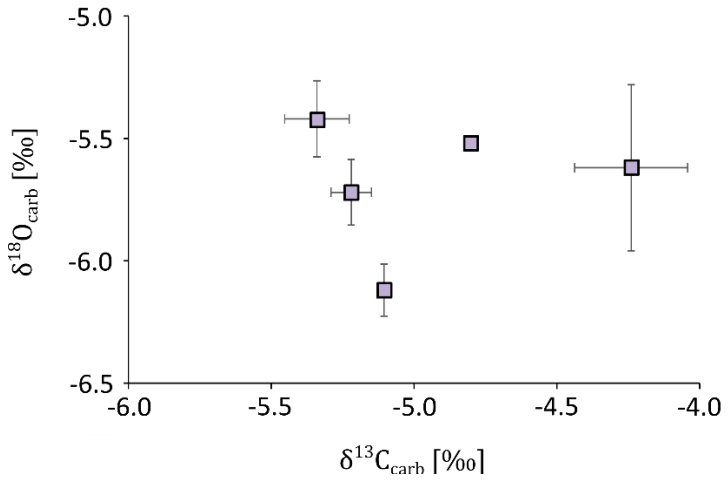

Figure 3: Cross-plot between $\delta^{13}C_{carb}$ and $\delta^{18}O_{carb}$ for carbonates detected during the Hirnantian at Dob's Linn. Slightly negative $\delta^{13}C_{carb}$ values indicate some of the carbonate carbon was derived from respired organic matter, consistent with early diagenetic carbonate formation. $\delta^{18}O_{carb}$ values are consistent with estimated subtropical seawater $\delta^{18}O$ values from the Hirnantian.

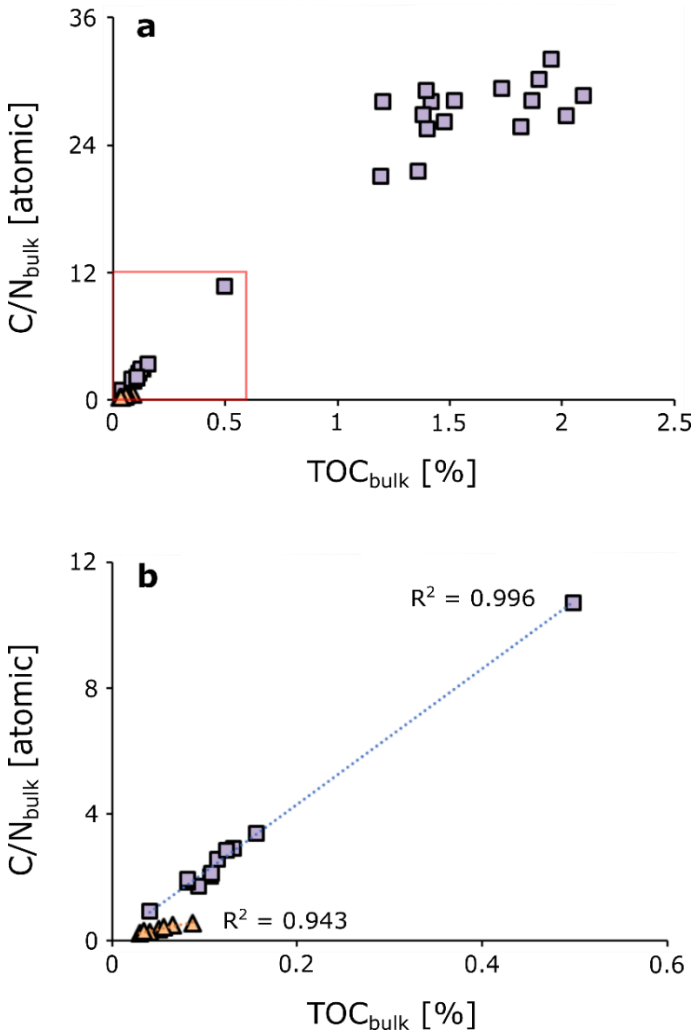

Figure 4: Relationship between bulk C_{org}/N ratios and TOC abundances for shales and bentonites (a) through the sampled Dob's Linn section and (b) zoomed in on samples from the Upper Hartfell Shale and all bentonite samples. Strong correlation in the Upper Hartfell and bentonite samples results from a large and invariable silicate-bound nitrogen fraction. A lower slope for the bentonite regression results from the larger silicate-bound nitrogen fraction held in the illite-enriched bentonite samples compared to the Upper Hartfell shale samples. Samples from the Lower Birkhill shale are more weakly correlated and more variable because as TOC increases, the organic nitrogen fraction makes up a larger percent of the total nitrogen, and variability in the organic C/N ratio starts to control the bulk C/N ratio. Symbols are as in Figure 2.

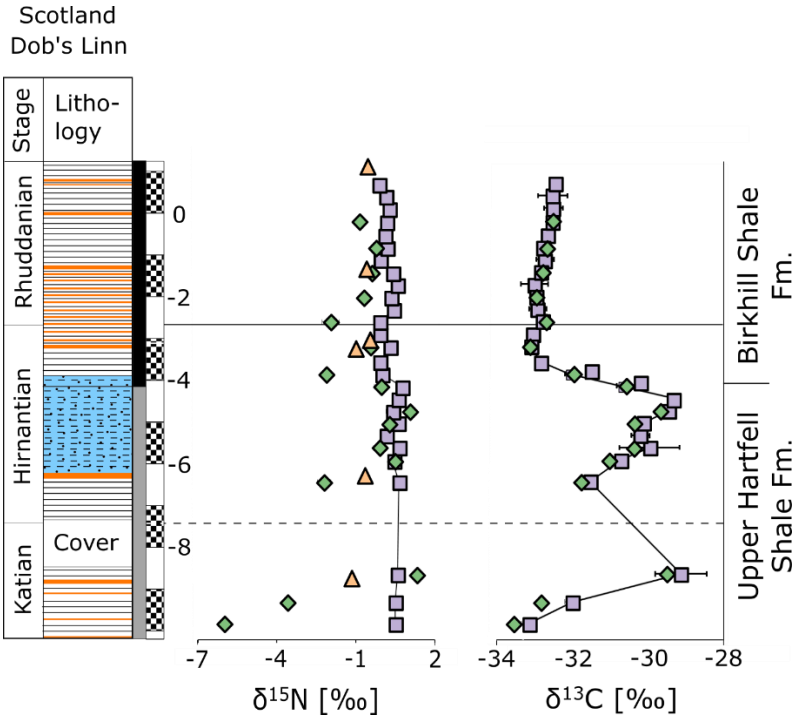

Figure 5: Nitrogen and carbon isotope chemostratigraphy through the Dob's Linn section. Nitrogen isotope values are fairly invariable through the section, suggesting persistent fixed nitrogen limitation at Dob's Linn. Carbon isotope values are consistent with prior studies of the Dob's Linn sediments, recording the Hirnantian positive carbon isotope excursion. Symbols are as in Figure 2.

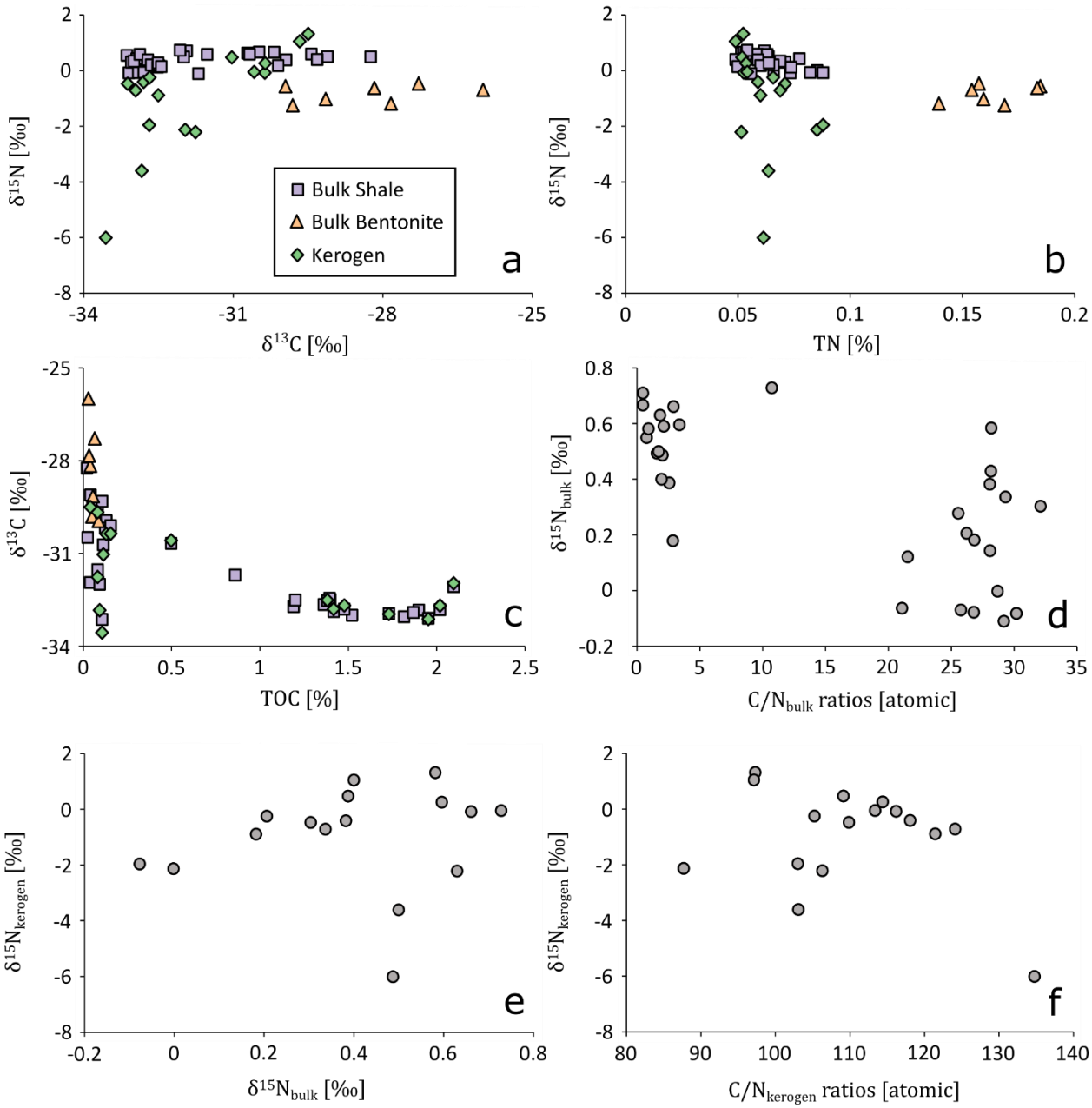

Figure 6: Cross-plots of nitrogen and carbon isotopes, abundances, and ratios from Dob's Linn shales, bentonites, and kerogen isolates. Grey circles compare kerogen to bulk rock data from the same samples. (a) Highlights the consistency of $\delta^{15}N$ values through the section save for a couple kerogen isolate measurements, (b) shows the relatively large silicate-bound nitrogen fraction in bentonite samples, and that there is no correlation between $\delta^{15}N$ values and total nitrogen, (c) shows the range of total organic carbon content in the section, and that there is no correlation between $\delta^{13}C$ values and TOC, (d) highlights the lack of a positive correlation between $\delta^{15}N_{bulk}$ values and C/N_{bulk} ratios suggesting limited metamorphic effects on $\delta^{15}N$ values, (e) shows general consistency between $\delta^{15}N_{bulk}$ values and $\delta^{15}N_{kerogen}$ values, and (f) highlights the lack of a positive correlation between $\delta^{15}N_{kerogen}$ values and $C/N_{kerogen}$ ratios further suggesting limited metamorphic and metasomatic effects on $\delta^{15}N$ values.

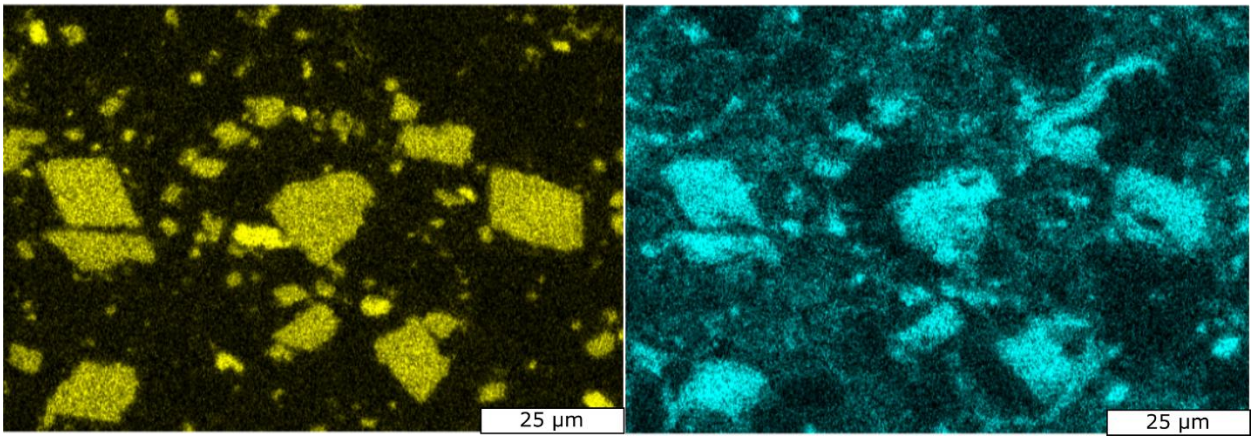

Figure 7: SEM-EDS maps of calcium (left) and magnesium (right). These maps are from the Dob's Linn Hirnantian sample -5.59, which is representative of our carbonate-bearing samples. The images reveal that the primary carbonate phase is polymodal, euhedral to subhedral dolomite, with subordinate calcite. Calcite appears as brighter yellow in the calcium image (left), with no corresponding signal in the magnesium image (right).

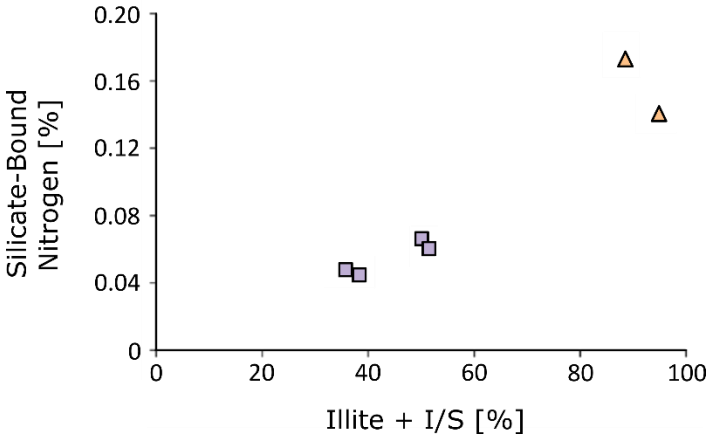

Figure 8: Percentage of illite plus illite/smectite vs. total silicate-bound nitrogen in shale and bentonite samples from Dob's Linn. Symbols are as in figure 2. Total bulk nitrogen percentages were used as an approximation of silicate-bound nitrogen in bentonite samples because organic-bound nitrogen concentrations in these samples are insignificant. The trend of increasing silicate-bound nitrogen with increasing illite abundance alludes to consistent ammonium concentrations in clay-proximal fluids during nitrogen sequestration into clays, through the Dob's Linn section.

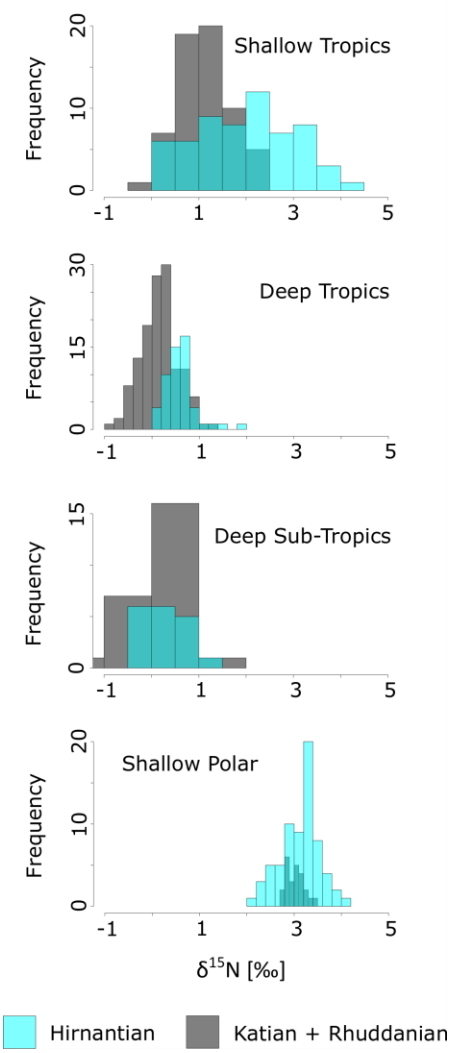

Figure 9: Histogram of nitrogen isotope values from the Katian to the Rhuddanian, separated by latitude and depositional environment. "Shallow tropics" contains the South China Nanbazi section (Luo et al., 2016), and the Canadian Truro Island and Eleanor Lake sections (Melchin et al., 2013), interpreted to have been deposited on a shallow marine shelf environment. "Deep tropics" contain the deep-shelf Wangjiawan section from South China (Luo et al., 2016) and the continental rise Vinini Creek section from the USA (LaPorte et al., 2009). "Deep sub-tropics" contains continental slope samples from this study at Dob's Linn, Scotland. "Shallow polar" comprises the Levin and Zadní Třebáň sections from the Czech Republic (Melchin et al., 2013). Notice the persistently high $\delta^{15}N$ values in the high latitude sections and the transiently enriched $\delta^{15}N$ values in the tropics during the Hirnantian, consistent with steeper latitudinal temperature gradients during the Hirnantian glaciation yielding slightly increased oxygen transport and nitrate concentrations towards the tropics.

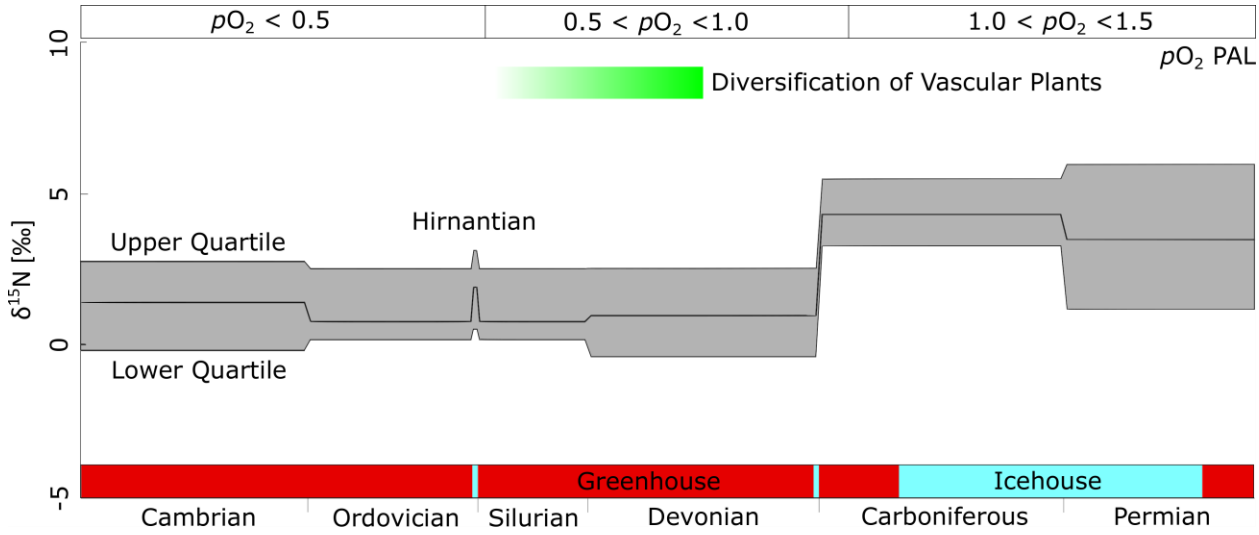

Figure 10: Compilation of marine sedimentary $\delta^{15}N$ values through the Paleozoic. Middle line of the grey shaded area represents the median of the data, and upper/lower quartiles are represented by the top and bottom of the grey shaded region, respectively. Data is binned by period, save for the Hirnantian age. Smaller temporal binning was avoided to mitigate the influence of low measurement/unit counts at any given time, and as a result the sharp transition of $\delta^{15}N$ values at the Devonian-Carboniferous boundary is an artifact of the binning. The number of measurements and units in this compilation are given in table 1. Icehouse-greenhouse transitions are highlighted as blue and red on the bottom bar, respectively. The top bar shows estimated ranges of atmospheric pO_2 (relative to present atmospheric level) (Krause et al., 2018). Green bar shows the diversification of vascular plants (Kenrick et al., 2012). The increase in global marine $\delta^{15}N$ values (and so marine nitrate concentrations) to near-modern levels of ~5‰ does not occur until the Carboniferous, after the diversification of vascular land plants and when atmospheric oxygen concentrations reach or exceed modern levels.

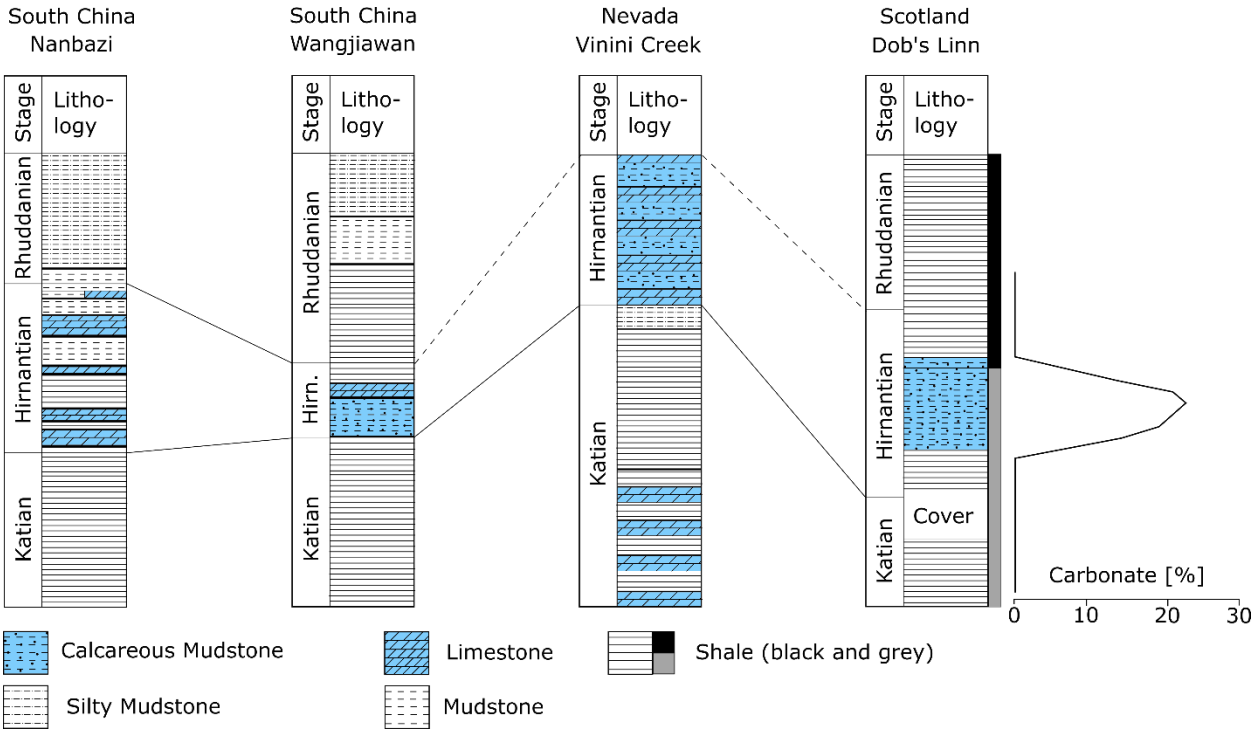

Figure 11: Stratigraphic sections showing carbonate deposition across the Hirnantian glaciation. Depositional environments and stratigraphic sections from the literature are as follows: Nanbazi – shallow shelf (Yan et al., 2009), Wangjiawan – deeper shelf (Chen et al., 1999), Vinini Creek – continental rise (Finney et al., 2007; Finney and Perry, 1991), Dob's Linn – continental slope (this study, Armstrong and Coe, 1997; Armstrong and Owen, 2002). The deposition of carbonaceous mudstone is restricted to the Hirnantian glaciation, consistent with a deepening of the carbonate compensation depth. Bentonite beds have been excluded from the Dob's Linn section for clarity.